*J. Fluid Mech.* (2002), *vol.* 467, *pp.* 331–359.  
DOI: 10.1017/S0022112002001465 Printed in the United Kingdom

# On nonlinear convection in mushy layers Part 1. Oscillatory modes of convection

By D. N. RIAHI

Department of Theoretical and Applied Mechanics, 216 Talbot Laboratory,
104 South Wright Street, University of Illinois at Urbana-Champaign, Urbana, IL 61801, USA

(Received 7 September 2001 and in revised form 15 April 2002)

We consider the problem of nonlinear convection in horizontal mushy layers during the solidification of binary alloys. We analyse the oscillatory modes of convection in the form of two- and three-dimensional travelling and standing waves. Under a near-eutectic approximation and the limit of large far-field temperature, we determine the solutions to the nonlinear problem by using a perturbation technique, and the stability of two- and three-dimensional solutions in the form of simple travelling waves, general travelling waves and standing waves is investigated. The results of the stability and the nonlinear analyses indicate that supercritical simple travelling rolls are stable over most of the studied range of parameter values, while supercritical standing rolls can be stable only over some small range of parameter values, where the simple travelling rolls are unstable. The results of the investigation of the onset of plume convection and chimney formation leading to the occurrence of freckles in the alloy crystal indicate that the chimney of the plume can be generated internally or near the lower boundary of the mushy layer. The roles of a Stefan number, a permeability parameter and a concentration ratio on the flow instability in both linear and nonlinear regimes are also determined.

## 1. Introduction

Recently Anderson & Worster (1996) considered the problem of convection during the solidification of a binary alloy in a horizontal mushy layer, analysed the linear stability of a motionless state and identified an oscillatory instability. Their investigation was based on a single-layer model of the mushy zone due to Amberg & Homsy (1993). A near-eutectic approximation was employed and the limit of large far-field temperature was considered. Such asymptotic limits allowed them to examine the dynamics of the mushy layer in the form of a small deviation from the classical system of convection in a horizontal porous layer of constant permeability. They also considered the limit of large Stefan number, which enabled them to reach the domain for the existence of the oscillatory instability.

The oscillatory instability detected by Anderson & Worster (1996) was based on a single-layer model in which the dynamics of the mushy layer were decoupled from the dynamics of the overlying liquid layer. Their oscillatory instability was distinct from that found by Chen, Lu & Yang (1994), which arose due to double-diffusive convection in a two-layer system in which stabilizing thermal buoyancy was present. The one-layer model treated in Anderson & Worster (1996) did not have double-diffusive effects, due to strong coupling between the solute and thermal fields, which was imposed by the condition of thermodynamic equilibrium. The oscillatory

instability discovered by Anderson & Worster (1996) was due to a mechanism internal to the mushy layer, similar to the oscillatory instability detected earlier by Sayre & Riahi (1995, 1997) in a linear and two-layer model and in the absence of any double-diffusive effect, and it implied the existence of an important interaction between convection and solidification within the mushy layer.

In the present investigation, we first revisit the linear model treated by Anderson & Worster (1996), and then extend that model to the nonlinear regime. We detect more dominant effects of the oscillatory modes of convection in the mushy layer and, through a stability analysis of the secondary solutions of the convective flow, determine the preferred flow pattern and the onset of plume convection, which can lead to chimney formation and the subsequent occurrence of freckles in the alloy crystal. Freckles are highly undesirable features since they are imperfections that can alter the material and mechanical properties of the solidified alloy.

The motivation of the present study is the desirability of understanding the qualitative features of the convective modes in the mushy layer and the onset of plume convection and formation of chimneys, so that, subsequently, ways to control the undesirable plume convection can be developed. For justification of the present analytical investigation of Amberg & Homsy's (1993) model, we refer the reader to their paper which provides convincing arguments about the complementary nature of the analytical studies of such model and the linear stability analysis of a more complete two-layer model, such as the one carried out by Worster (1992), and the fully numerical simulation of a more sophisticated mushy layer system (Neilson & Incropera 1993).

Few analytical investigations have been carried out so far on nonlinear convection in a mushy layer. Amberg & Homsy (1993) developed a single-layer model for convection in a horizontal mushy layer which focuses on the mushy-layer mode of convection, which is one of the two primary modes of convection discovered earlier by Worster (1992) in a two-layer system. Amberg & Homsy (1993) made a number of simplifying assumptions including both the thickness of the layer and the departure from the eutectic point being small and the mushy layer being isolated from the overlying liquid layer. Among the non-dimensional parameters of their model, a Stefan number $S_t$, representing the latent heat release due to solidification, turns out to play a significant role in the realization of the non-oscillatory or oscillatory nature of the mode of convection in the mushy layer. Amberg & Homsy (1993) considered only order-one values of $S_t$ in their study. However, as already noted by Anderson & Worster (1996), for such values of $S_t$, no oscillatory mode of convection are found at the onset of motion, whereas they are found for large values of $S_t$. This result has also been confirmed by our calculation in the present study. Amberg & Homsy's model describes correctly the coupling between the flow and re-melting for the nonlinear mushy-layer mode, which is thought to be responsible for the chimney formation. Amberg & Homsy (1993) rescaled the variables and the Rayleigh number appropriately and restricted their analysis to the case where the mushy-layer thickness $\delta$ is of order of the amplitude $\varepsilon$ of convection. They employed a weakly nonlinear analysis and calculated solutions in the form of two-dimensional steady rolls to order $\varepsilon^2$ and steady hexagons to order $\varepsilon$. They found that either sub- or supercritical steady rolls are possible and steady hexagons can be transcritical.

Anderson & Worster (1995) extended the weakly nonlinear analysis of Amberg & Homsy (1993) to the limit of large $S_t$ and the case $\varepsilon \ll \delta \ll 1$. They applied a double-series expansion in powers of $\varepsilon$ and $\delta$ for the rescaled variables and the Rayleigh number. They focused on the steady modes of convection and calculated

the steady solutions in the form of two-dimensional rolls and hexagons, and analysed the stability of these solutions using the evolution equation that they derived for small-amplitude coefficients of such solutions. They found that rolls or hexagons, with either up-flow or down-flow at the cell centres, could be stable, depending on the relative strengths of different physical mechanisms.

The present paper studies the oscillatory modes of convection in mushy layers using Amberg & Homsy's (1993) model in its extended form as studied by Anderson & Worster (1995). We employ weakly nonlinear and stability analyses to determine the finite-amplitude oscillatory solutions and their stability with respect to arbitrary three-dimensional disturbances. The objectives of the analysis are to isolate the nonlinear properties of the oscillatory modes of the compositional convection in the mushy layers for various values of the parameters and to determine the preferred flow features and structures near the onset of plume convection and chimney formation. We have found a number of interesting results. In particular, depending on the values of the parameters, either simple travelling rolls in the form of either right-travelling rolls (where the phase velocity of the rolls is in the direction of the component of the position vector along the wavenumber vector) or left-travelling rolls, (where the phase velocity of the rolls is in the direction opposite to that of the component of the position vector along the wavenumber vector) or standing rolls can be stable. The stable travelling and standing rolls were found to be supercritical.

Our study complements the previous nonlinear study of non-oscillatory convection in mushy layers by Anderson & Worster (1995). We noted that, at the relevant scaling established by Anderson & Worster (1995, 1996), the linear system of the problem exhibits both stationary and oscillatory modes of convection at comparable critical values of the Rayleigh number for the onset of convection. Hence, to determine valid analytical results, which could also be compared with the available experimental results (Tait, Jahrling & Jaupart 1992), a nonlinear theory needed to be developed and analysed, which could account for both stationary and oscillatory modes of convection (Riahi 2002). However, prior to the present study, no nonlinear investigation of oscillatory convection alone in mushy layers had been carried out, and, thus, to understand its qualitative features the present investigation was necessary. The present paper is part 1 of a comprehensive nonlinear study of oscillatory and stationary modes of convection in mushy layers. Part 2 of the study (Riahi 2002) takes into account the combination of both oscillatory and non-oscillatory modes, in order to arrive at a reasonably complete theory for the present problem.

Recently Chung & Chen (2000) considered the mushy layer treated by Anderson & Worster (1995) but for a constant pressure condition at the upper boundary instead of the original impermeable upper boundary condition. They carried out essentially the same type of analysis, procedure and method of approach as Anderson & Worster (1995) to determine the steady solutions for rolls and hexagons. The constant pressure condition at the upper boundary improves the model quantitatively, as was shown by Chung & Chen (2000), since with it the mushy layer model of Amberg & Homsy (1993) becomes closer to the more complete two-layer model of an actual solidification system, which, in particular, allows inflow and outflow through the mush–liquid interface. However, no significant qualitative improvement of the results was expected as is evident from the results due to Chung & Chen (2000). Like Anderson & Worster (1995) we consider the model with the impermeable upper boundary condition. We did not employ the permeable upper boundary condition, such as the condition $\partial w/\partial z = 0$ used by Chung & Chen (2000), for three main reasons. First, as is evident from the work of these latter authors, the permeable

upper boundary condition for the mushy layer model complicates the analytical procedure to determine the solutions, and it amplifies the other complications, which arise as a result of the oscillatory nature of the modes. Secondly, as is often the case in the classical convection system, there is no evidence that any new significant qualitative result can be obtained by such a change in the upper boundary condition. Thirdly, we were interested only in determining the qualitative features of the results. Thus, as in the case of the very recent study by Guba (2001) and as discussed earlier by Anderson & Worster (1995, 1996), Amberg & Homsy's simpler model, which can provide reliable qualitative predictions, was found to be quite suitable and appropriate for our investigation.

In regard to the prediction of the available experimental results (Tait *et al.* 1992), it should be noted that no theoretical studies have yet predicted the preference of down-hexagons in the same parameter regime as observed by Tait *et al.* (1992). Although the quantitative results reported in Chung & Chen (2000) indicated that the domain of stable down-hexagons was enlarged compared to the corresponding domain determined by Anderson & Worster (1995), the main disagreement with the experimental result of Tait *et al.* (1992) still persisted. Chung & Chen (2000) predicted stable up-hexagons in the parameter regime where Tait *et al.* (1992) observed stable down-hexagons. The reason for this inconsistency, for steady convection and based on the single-layer models, is not known at present, but it could be due to factors such as the near-eutectic approximation, the large far-field temperature limit, the exclusion of the overlying liquid layer, the prescribed constrained growth at constant solidification rate and the exclusion of the oscillatory modes. As is explained further in the § 6, the investigation of part 2, which will take into account combination of both oscillatory and stationary modes of convection, is expected to indicate enlargement of the domain for the preference of down-hexagons.

The following three sections 2–4 deal with the mathematical formulation of the problem, the general description of the nonlinear oscillatory convection and the stability analysis. The results of the oscillatory solutions are presented and discussed in § 5, which is followed by the conclusion and some remarks in § 6.

## 2. Mathematical formulation

We consider a binary alloy melt that is cooled from below and solidified at a constant speed $V_0$. Following Amberg & Homsy (1993) and Anderson & Worster (1995), we consider a horizontal mushy layer of thickness $d$ adjacent to and above the solidification front to be physically isolated from the overlying liquid and underlying solid zones. The overlying liquid is assumed to have a composition $C_0 > C_e$ and temperature $T_\infty > T_L(C_0)$ far above the mushy layer, where $C_e$ is the eutectic temperature, $T_L(\tilde{C})$ is the liquidus temperature of the alloy and $\tilde{C}$ is the composition. It is thus assumed that the mushy layer is bounded from above and below by rigid and isothermal boundaries. We consider the solidification system in a moving frame of reference $o\tilde{x}\tilde{y}\tilde{z}$, whose origin lies on the solidification front and translating at the speed $V_0$ with the solidification front in the positive $\tilde{z}$-direction.

It should be noted that no double-diffusive effect is present in the above-described one-layer mushy-zone model since such a mushy layer is assumed to be in local thermodynamic equilibrium and, thus,

$$T = T_L(C_0) + M(\tilde{C} - C_0),$$

where $T$ is the temperature and $M$ is the slope of the liquidus (Anderson & Worster

1996). The mushy layer is treated as a porous layer (Fowler 1985; Worster 1992), where the solid dendrites and the liquid coexist, and Darcy's law is used.

Next, we consider the equations for momentum, continuity, heat and solute for the flow of melt in the mushy layer in the moving frame described above. These equations are non-dimensionalized by using $V_0, k/V_0, k/V_0^2$, $\beta\Delta C\rho g k/V_0$, $\Delta C$ and $\Delta T$ as scales for velocity, length, time, pressure, solute and temperature, respectively. Here $k$ is the thermal diffusivity, $\rho$ is a reference (constant) density, $\beta = \beta^* - M\alpha^*$, where $\alpha^*$ and $\beta^*$ are the expansion coefficients for the heat and solute, respectively, and $M$ is assumed to be constant, $\Delta C = C_0 - C_e$, $\Delta T = T_L(C_0) - T_e$ and $T_e$ is the eutectic temperature. The non-dimensional form of the equations for momentum, continuity, temperature and solute concentration in the mushy layer are (Worster 1992)

$$K(\tilde{\phi})\boldsymbol{u} = -\nabla\tilde{P} - \tilde{R}\tilde{\theta}\boldsymbol{z}, \tag{1a}$$

$$\nabla\cdot\boldsymbol{u} = 0, \tag{1b}$$

$$\left(\frac{\partial}{\partial\tilde{t}} - \frac{\partial}{\partial\tilde{z}}\right)(\tilde{\theta} - S_t\tilde{\phi}) + \tilde{\boldsymbol{u}}\cdot\nabla\tilde{\theta} = \nabla^2\tilde{\theta}, \tag{1c}$$

$$\left(\frac{\partial}{\partial\tilde{t}} - \frac{\partial}{\partial\tilde{z}}\right)[(1-\tilde{\phi})\tilde{\theta} + C_r\tilde{\phi}] + \tilde{\boldsymbol{u}}\cdot\nabla\tilde{\theta} = 0, \tag{1d}$$

where $\tilde{\boldsymbol{u}} = \tilde{u}\boldsymbol{x} + \tilde{v}\boldsymbol{y} + \tilde{w}\boldsymbol{z} = (1-\tilde{\phi})\boldsymbol{U}$ is the volume flux per unit area (Joseph 1976), $\boldsymbol{U}$ is the velocity vector, $\tilde{u}$ and $\tilde{v}$ are the horizontal components of $\boldsymbol{u}$ in the $\tilde{x}$- and $\tilde{y}$-directions, respectively, $\boldsymbol{x}$ and $\boldsymbol{y}$ are unit vectors in the positive $\tilde{x}$- and $\tilde{y}$-directions, $\tilde{w}$ is the vertical component of $\boldsymbol{u}$ in the $\tilde{z}$-direction, $\boldsymbol{z}$ is a unit vector in the positive $\tilde{z}$-direction, $\tilde{P}$ is the modified pressure, $\tilde{\theta}$ is the non-dimensional composition, or equivalently temperature (Worster 1992), $\theta = [T - T_L(C_0)]/\Delta T = (\tilde{C} - C_0)/\Delta C$, $\tilde{t}$ is the time variable, $\tilde{\phi}$ is the local solid fraction, $\tilde{R} = \beta\Delta C g\Pi(0)/(V_0\nu)$ is the Rayleigh number, $\Pi(0)$ is reference value at $\tilde{\phi} = 0$ of the permeability $\Pi(\tilde{\phi})$ of the porous medium, which is assumed to be finite (Worster 1992), $\nu$ is the kinematic viscosity, $g$ is acceleration due to gravity, $K(\tilde{\phi}) \equiv \Pi(0)/\Pi(\tilde{\phi})$, $S_t = L/(C_L\Delta T)$ is the Stefan number, $C_L$ is the specific heat per unit volume, $L$ is the latent heat of solidification per unit volume, $C_r = (C_s - C_0)/\Delta C$ is a concentration ratio, and $C_s$ is the composition of the solid-phase forming the dendrites. Equation (1$d$) is based on the limit of sufficiently large value of the Lewis number $k/k_s$ (Worster 1992; Anderson & Worster 1995), where $k_s$ is the solute diffusivity.

The governing equations (1$a$)–(1$d$) are subject to the boundary conditions (Amberg & Homsy 1993)

$$\tilde{\theta} + 1 = \tilde{w} = 0 \quad \text{at} \quad \tilde{z} = 0, \tag{2a}$$

$$\tilde{\theta} = \tilde{w} = \tilde{\phi} = 0 \quad \text{at} \quad \tilde{z} = \delta, \tag{2b}$$

where $\delta = dV_0/k$ is a growth Péclet number representing the dimensionless depth of the layer.

Following Anderson & Worster (1995, 1996), in reducing the model asymptotically we assume the following rescaling in the limit of sufficiently small $\delta$:

$$C_r = C/\delta, \quad S_t = S/\delta, \quad \varepsilon \ll \delta \ll 1, \tag{3a}$$

$$(\tilde{x}, \tilde{y}, \tilde{z}) = \delta(x, y, z), \quad \tilde{t} = \delta^2 t, \quad R^2 = \delta\tilde{R}, \tag{3b}$$

$$\tilde{\theta} = \theta_B(z) + \varepsilon\theta(x, y, z, t), \tag{3c}$$

$$\tilde{\phi} = \phi_B(z) + \varepsilon\phi(x, y, z, t), \tag{3d}$$

$$\tilde{\boldsymbol{u}} = 0 + (\varepsilon R/\delta)\,\boldsymbol{u}(x, y, z, t), \tag{3e}$$

$$\tilde{P} = RP_B(z) + R\varepsilon P(x, y, z, t), \tag{3f}$$

where $C$ and $S$ are order-one quantities as $\delta \to 0$, and the quantities with subscript '$B$' are the basic flow variables for the motionless state, which are assumed to be a function of $z$ only. The small deviation of each dependent variable from its basic state is measured by a perturbation amplitude $\varepsilon$ and can vary with respect to the horizontal, vertical and time variables as shown in (3$c$)–(3$f$).

As discussed in Anderson & Worster (1995, 1996), the assumption of thin mushy layer ($\delta \ll 1$) is associated with large non-dimensional far-field temperature $\theta_{\infty=}[T_\infty - T_L(C_0)]/\Delta T \gg 1$, which can occur when the initial $\tilde{C}$ is close to $C_e$. The assumption of order-one $C$ corresponds to the near–eutectic approximation (Fowler 1985), which allows one to describe the mushy layer as a porous layer of constant permeability to the leading order. The assumption of order-one $S$ allowed Anderson & Worster (1996) to detect an oscillatory instability from their linear model.

The rescalings (3$a$)–(3$f$) are then used in (1$a$)–(1$d$) and (2$a$)–(2$b$). This system of equations and boundary conditions admits a motionless basic state, which is steady and horizontally uniform. The basic-state solution in terms of asymptotic expansions for $\delta \ll 1$ is

$$\theta_B = (z-1) + \delta(z - z^2)G/2 + \cdots, \quad G \equiv 1 + S/C, \tag{4a}$$

$$\phi_B = \delta(1-z)/C + \delta^2[-(1-z)^2/C^2 + (z^2 - z)G/(2C)] + \cdots, \tag{4b}$$

$$P_B = P_0 + R[(z - z^2/2) + \delta(z^2/2 - z^3/3)G/2 + \cdots], \tag{4c}$$

where $P_0$ is a constant. Since $\tilde{\phi}$ is expected to be small, according to (4$b$), the following expansion for $K(\tilde{\phi})$ will be implemented later in the governing system:

$$K(\tilde{\phi}) = 1 + K_1\tilde{\phi} + K_2\tilde{\phi}^2 + \cdots, \tag{5}$$

where $K_1$ and $K_2$ are constants (Amberg & Homsy 1993).

For the analysis to be presented in the next section, it is convenient to use the general representation

$$\boldsymbol{u} = \boldsymbol{\Omega} V + \boldsymbol{E}\Psi, \tag{6a}$$

$$\boldsymbol{\Omega} = \nabla \times \nabla \times \boldsymbol{z}, \quad \boldsymbol{E} = \nabla \times \boldsymbol{z}, \tag{6b}$$

for the divergent–free vector field $\boldsymbol{u}$ (Chandrasekhar 1961). Here $V$ and $\Psi$ are the poloidal and toroidal functions for $\boldsymbol{u}$, respectively. By taking the vertical component of the curl of (1$a$) it can be shown that the toroidal part $\boldsymbol{E}\Psi$ of $\boldsymbol{u}$ must vanish. Taking the vertical component of the double curl of (1$a$) and using (1$b$) in (1)–(2), we find the following system, which will be analysed in the next section:

$$\nabla^2[K(\phi_B + \varepsilon\phi)\Delta_2 V] + \left(\frac{\partial}{\partial z}\right)[\boldsymbol{\Omega} V \cdot \nabla K(\phi_B + \varepsilon\phi)] - R\Delta_2\theta = 0, \tag{7a}$$

$$\left(\frac{\partial}{\partial t} - \delta\frac{\partial}{\partial z}\right)\left(-\theta + \frac{S\phi}{\delta}\right) + R\left(\frac{\mathrm{d}\theta_B}{\mathrm{d}z}\right)\Delta_2 V + \nabla^2\theta = \varepsilon R\boldsymbol{\Omega} V \cdot \nabla\theta, \tag{7b}$$

$$\left(\frac{\partial}{\partial t} - \delta\frac{\partial}{\partial z}\right)\left[(-1 + \phi_B)\theta + \theta_B\phi + \varepsilon\phi\theta - \frac{C\phi}{\delta}\right] + R\left(\frac{\mathrm{d}\theta_B}{\mathrm{d}z}\right)\Delta_2 V = \varepsilon R\boldsymbol{\Omega} V \cdot \nabla\theta, \tag{7c}$$

$$\theta = V = 0 \quad \text{at} \quad z = 0, \tag{7d}$$

$$\theta = V = \phi = 0 \quad \text{at} \quad z = 1, \tag{7e}$$

where

$$\Delta_2 \equiv \frac{\partial^2}{\partial x^2} + \frac{\partial^2}{\partial y^2}.$$

## 3. Weakly nonlinear analysis

In this section we perform a weakly nonlinear analysis, based on double series expansions in powers of two small parameters for the perturbation quantities, of the type carried out by Busse (1967) and Busse & Riahi (1980). Here the two small parameters are $\delta$ and $\varepsilon$ which satisfy the condition given in (3*a*). Following Anderson & Worster (1995), we first make a formal asymptotic expansion in $\varepsilon \ll 1$ and then at each order in $\varepsilon$ make a formal asymptotic expansion in $\delta \ll 1$. Since we shall investigate the oscillatory modes of convection, the appropriate expansions are for the dependent variables of the perturbation system, $R$ and the frequency $\omega$ of the oscillatory modes of convection (Riahi 1992). These expansions are

$$\begin{aligned}(V,\theta,\phi,R,\omega) = {} & [(V_{00}+\delta V_{01}+\cdots),(\theta_{00}+\delta\theta_{01}+\cdots),(\phi_{00}+\delta\phi_{01}+\cdots),\\ & (R_{00}+\delta R_{01}+\cdots),(\omega_{00}+\delta\omega_{01}+\cdots)]+\varepsilon[(V_{10}+\delta V_{11}+\cdots),\\ & (\theta_{10}+\delta\theta_{11}+\cdots),(\phi_{10}+\delta\phi_{11}+\cdots),(R_{10}+\delta R_{11}+\cdots),\\ & (\omega_{10}+\delta\omega_{11}+\cdots)]+\varepsilon^2[(V_{20}+\delta V_{21}+\cdots),(\theta_{20}+\delta\theta_{21}+\cdots),\\ & (\phi_{2(-1)}/\delta+\phi_{20}+\delta\phi_{21}+\cdots),(R_{20}+\delta R_{21}+\cdots),\\ & (\omega_{20}+\delta\omega_{21}+\cdots)]+\cdots, \end{aligned} \tag{8}$$

where, as in the case of steady modes (Anderson & Worster 1995), the expansion of $\phi$ is singular at order $\varepsilon^2$ as $\delta \to 0$, but it turns out that $O(1/\delta)$ is needed only in the stability analysis of the next section since the $O(\varepsilon^2)$ problem is found to be forced by a term of $O(1/\delta)$ in the solute equation for the disturbances.

Upon inserting (8) into (7*a*)–(7*e*) and disregarding the nonlinear terms, we find the linear problem which we analysed in direct analogy to that carried out by Anderson & Worster (1996). Hence, no details will be provided here and, instead, the main results on the neutral boundary are given. At order $1/\delta$ we find $\omega_{00} = 0$. At order $\delta^0$ we find

$$V_{00} = [(\pi^2+a^2)/(R_{00}a^2G)]\sin(\pi z)\sum_{n=-N}^{N}(A_n^+\eta_n^+ + A_n^-\eta_n^-), \tag{9a}$$

$$\theta_{00} = -\sin(\pi z)\sum_{n=-N}^{N}(A_n^+\eta_n^+ + A_n^-\eta_n^-), \tag{9b}$$

$$\phi_{00} = \sum_{n=-N}^{N}[f_n(z)A_n^+\eta_n^+ + f_n^*(z)A_n\eta_n^-], \eta_n^{\pm} \equiv \exp[\mathrm{i}(\boldsymbol{a}_n\cdot\boldsymbol{r} \pm S_n\omega t)], \tag{9c}$$

$$R_{00}^2 = (\pi^2+a^2)^2/(a^2G), \tag{9d}$$

where

$$f_n(z) = (\mathrm{i}\omega_{01}S_n/\pi)\sin(\pi z) + \cos(\pi z) + \exp[\mathrm{i}\omega_{01}S_n(z-1)] \tag{9e}$$

and

$$S_n \equiv 1 \quad \text{for} \quad n>0 \quad \text{and} \quad -1 \quad \text{for} \quad n<0. \tag{9f}$$

Here i is the pure imaginary number (i $\equiv \sqrt{-1}$), subscript '$n$' takes only non-zero integer values from $-N$ to $N$, $N$ is a positive integer representing the number of distinct modes, $\boldsymbol{r}$ is the position vector, and the horizontal wavenumber vectors $\boldsymbol{a}_n$ satisfy the properties

$$\boldsymbol{a}_n \cdot \boldsymbol{z} = 0, \quad |\boldsymbol{a}_n| = a, \quad \boldsymbol{a}_{-n} = -\boldsymbol{a}_n. \tag{10}$$

The coefficients $A_n^+$ and $A_n^-$ satisfy the conditions

$$\sum_{n=-N}^{N} (A_n^+ A_n^{+*} + A_n^- A_n^{-*}) = 2, \quad A_n^{\pm *} = A_{-n}^{\pm}, \tag{11}$$

where the asterisk indicates the complex conjugate. Minimizing the expression for $R_{00}$, given in (9$d$), with respect to the wavenumber $a$, we find

$$R_{00c} = 2\pi/\sqrt{G}, \quad a_c = \pi. \tag{12}$$

In all the analyses and solutions to follow we shall set $R_{00} = R_{00c}$ and $a = a_c$, unless indicated otherwise. Due to the complexity of the present oscillatory problem, we consider a simplifying assumption by following Anderson & Worster (1995) and focusing on a particular limiting case where $K_1$ is small, and, in particular, we assume that $K_1$ is of order $\varepsilon$. At order $\delta$ we find the solutions $V_{01}$, $\theta_{01}$ and $\phi_{01}$, whose expressions are very lengthy and are not given in this paper. The real and imaginary parts of the solvability condition at this order yield

$$R_{01} = 2\pi G_t \sqrt{G}[1/4 + \pi^2(1 + \cos\omega_{01})/(\pi^2 - \omega_{01}^2)^2], \tag{13a}$$

$$\omega_{01}\{1 + [2\pi^2 G_t/(\pi^2 - \omega_{01}^2)][1 - 2\pi^2 \sin\omega_{01}/(\pi^2\omega_{01} - \omega_{01}^3)]\} = 0, \tag{13b}$$

where

$$G_t \equiv (G - 1)/(CG^2). \tag{13c}$$

### 3.1. *Travelling waves*

Next, we analyse the nonlinear problem for the travelling waves. At order $\varepsilon/\delta$, we find $\omega_{10} = 0$. At order $\varepsilon$ the system (7$a$)–(7$e$) can be reduced to the form given by (A1) in Appendix A. The solvability conditions for the nonlinear systems require the following special travelling wave solutions $V_{00n}^{\pm}$ and $\theta_{00n}^{\pm}$ of the linear system:

$$(V_{00n}^{\pm}, \theta_{00n}^{\pm}) = [1/(\pi\sqrt{G}), -1]\sin(\pi z)(A_n^{\pm}\eta_n^{\pm} + \text{c.c.}), \tag{14}$$

where 'c.c.' indicates the complex conjugate of the preceding expression. It turns out that there is no need to consider a special linear solution for $\phi$ since the governing nonlinear systems are usually reduced to a form where only (14) will be needed to form the corresponding solvability conditions. Multiplying (A 1$a$) by $GV_{00n}^{\pm}$, (A 1$b$) by $\theta_{00n}^{\pm}$, adding, applying the boundary conditions, averaging over the whole layer and taking a time average over period $2\pi/\omega_{01}$ yields

$$2|A_n^{\pm}|^2 R_{10} = \langle \theta_{00n}^{\pm} \boldsymbol{\Omega} V_{00} \cdot \nabla\theta_{00} \rangle, \tag{15}$$

where an angular bracket indicates a total average over the layer and in time. The right-hand side of (15) for $R_{10}$ consists of sum of terms involving integrals of the form $\langle \eta_n^{\pm}\eta_l^{\pm}\eta_p^{\pm} \rangle$, which are all zero, due to the time averaging, since each mode is oscillatory in time. Hence $R_{10} = 0$. By the same reasoning, the solvability conditions for the system at order $\varepsilon\delta$ also yield $R_{11} = \omega_{11} = 0$. The solution to the system (A1) is given

by (A 2). The solution to the system at orders $\varepsilon\delta$ involves very lengthy expressions and will not be given in this paper.

The solvability conditions for the system at order $\varepsilon^2/\delta$ yield $\omega_{20} = 0$.

At order $\varepsilon^2$ the system (7*a*)–(7*e*) can be reduced to the form given by (A 3). The simplified forms of the solvability conditions for (A 3) yield

$$\begin{aligned} 2R_{20}|A_n^+|^2 = \sum_{m=-N}^{N} \{ & (T_{nm}^{(1)} + T_{-n,m}^{(1)})|A_n^+|^2|A_m^+|^2 + [T_{nm}^{(2)} A_n^- A_{-n}^+ \delta(S_m - S_n) \\ & + T_{-n,m}^{(2)} A_{-n}^- A_n^+ \delta(S_m + S_n)] A_m^+ A_{-m}^- + (T_{nm}^{(3)} + T_{-n,m}^{(3)})|A_n^+|^2|A_m^-|^2 \\ & + [T_{nm}^{(4)} A_n^- A_{-n}^+ \delta(S_m + S_n) + T_{-n,m}^{(4)} A_{-n}^- A_n^+ \delta(S_m - S_n)] A_m^- A_{-m}^+ \}, \end{aligned} \tag{16a}$$

$$\begin{aligned} 2R_{20}|A_n^-|^2 = \sum_{m=-N}^{N} \{ & [T_{nm}^{(5)} A_n^+ A_{-n}^- \delta(S_m - S_n) + T_{-n,m}^{(5)} A_{-n}^+ A_n^- \delta(S_m + S_n)] A_m^- A_{-m}^+ \\ & + (T_{nm}^{(7)} + T_{-n,m}^{(7)})|A_n^-|^2|A_m^-|^2 + [T_{nm}^{(6)} A_n^+ A_{-n}^- \delta(S_m + S_n) + T_{-n,m}^{(6)} A_{-n}^+ A_n^- \delta \\ & \times (S_m - S_n)] A_m^+ A_{-m}^- + (T_{nm}^{(8)} + T_{-n,m}^{(8)})|A_n^-|^2|A_m^+|^2 \}, \end{aligned} \tag{16b}$$

where

$$\delta(S) = 1 \quad \text{for} \quad S = 0 \quad \text{and} \quad 0 \quad \text{for} \quad S \neq 0, \tag{16c}$$

and the expressions for $T_{nm}^{(i)}$ $(i = 1, \ldots, 8)$ are given by (A 4*a*)–(A 4*h*).

The first equation in (11) and (16*a*)–(16*b*) form a system of $(4N + 1)$ equations for $(4N + 1)$ unknowns $A_n^+$, $A_n^-$ and $R_{20}$ $(n = -N, \ldots, -1, 1, \ldots, N)$. This system can be used to study the solutions in the form of travelling waves, where $A_n^+ \neq A_n^-$ for at least one $n$.

*Simple travelling waves*

The left-(right-) travelling wave solutions of (11) and (16*a*)–(16*b*) are given below in the so-called 'regular' case, in which all angles between two neighbouring $\boldsymbol{a}$-vectors are equal:

$$\left.\begin{aligned} & |A_1^-| = \cdots = |A_N^-| = 0 (|A_1^+| = \cdots = |A_N^+| = 0), \\ & |A_1^+|^2 = \cdots = |A_N^+|^2 = 1/N (|A_1^-|^2 = \cdots = |A_N^-|^2 = 1/N), \\ & 2R_{20}^{(st)} = (1/N) \sum_{m=1}^{N} (T_{1m}^{(st)} + T_{1,-m}^{(st)}), \end{aligned}\right\} \tag{17a}$$

where $R_{20}^{(st)}$ denotes the expression for $R_{20}$ for these simple travelling wave solutions and

$$T_{nm}^{(st)} = T_{nm}^{(1)} + T_{-n,m}^{(1)}. \tag{17b}$$

Solutions (17*a*) also hold for the so-called 'semi-regular' type solutions, where the scalar product between any one of the $\boldsymbol{a}$-vectors and its two neighbouring $\boldsymbol{a}$-vectors assumes the constant values $\alpha_1$ and $\alpha_2$. Regular solutions follow from the semi-regular ones for the special case $\alpha_1 = \alpha_2$ (Busse 1967). The simplest form of such solutions corresponds to the case of left-(right-) travelling rolls where

$$N = 1, \quad R_{20}^{(st)} = (1/2)(T_{11}^{(st)} + T_{1,-1}^{(st)}), \quad |A_1^+|^2 = 1 (|A_1^-|^2 = 1). \tag{18}$$

As indicated by (17$a$) and (18) and consistent with the symmetry property of the present problem, the expression for $R_{20}^{(st)}$ for the left-travelling waves is the same as that for the right-travelling waves.

*General travelling waves*

The semi-regular solutions of (16$a$) and (16$b$) for the case of general travelling waves are

$$\left.\begin{aligned} A_1^+ &= \cdots = A_N^+ = [(0.5-b)/N]^{0.5}, \quad A_1^- = \cdots = A_N^- = [(0.5+b)/N]^{0.5}, \\ R_{20}^{(gt)} &= \{R_{20}^{(st)}[(0.5+b)^{1.5} + (0.5-b)^{1.5}]/[(0.5+b)^{0.5} \\ &\quad + (0.5-b)^{0.5}]\} + (0.25-b^2)^{0.5}(2R_{20}^{(s)} - R_{20}^{(st)}), \end{aligned}\right\} \tag{19a}$$

where $b$ is a positive constant in the range

$$-0.5 < b < 0.5, \tag{19b}$$

whose value specifies the particular travelling wave solution. Here $R_{20}^{(gt)}$ and $R_{20}^{(s)}$ denote, respectively, the expressions for $R_{20}$ for such solutions in the cases of a general travelling wave and standing wave. The expression for $R_{20}^{(s)}$ will be given in the next subsection. It can be seen from (19$a$) that, as expected, $R_{20}^{(gt)} = R_{20}^{(s)}$ for $b = 0$, and $R_{20}^{(gt)} = R_{20}^{(st)}$ in the limit of either $b = -0.5$ or $b = 0.5$.

### 3.2. *Standing waves*

The analysis provided in the previous subsection for the travelling waves can be carried out in a similar manner for the standing waves, which is briefly presented in the following paragraphs.

For the standing wave solutions, where $A_n^+ = A_n^-$ for every $n$, the special linear solution, which is used to form the solvability conditions, must itself be standing wave of the form

$$(V_{00n}, \theta_{00n}) = (V_{00n}^+ + V_{00n}^-, \theta_{00n}^+ + \theta_{00n}^-), A_n^+ \equiv A_n^- \equiv A_n, \tag{20}$$

instead of (14). Consequently, the resulting solvability conditions at orders $\varepsilon/\delta$, $\varepsilon$, $\varepsilon^2/\delta$ and $\varepsilon^2$ yield, respectively, $\omega_{10} = 0$, $R_{10} = 0$, $\omega_{20} = 0$ and

$$\begin{aligned} 4A_nR_{20} = \sum_{m=-N}^{N} \{&(T_{nm}^{(1)} + T_{-n,m}^{(1)} + T_{nm}^{(3)} + T_{-n,m}^{(3)} + T_{nm}^{(7)} + T_{-n,m}^{(7)} + T_{nm}^{(8)} + T_{-n,m}^{(8)}) \\ &+ (T_{nm}^{(2)} + T_{-n,m}^{(4)} + T_{nm}^{(5)} + T_{-n,m}^{(6)})\delta(S_m - S_n) + (T_{-n,m}^{(2)} + T_{nm}^{(4)} + T_{-n,m}^{(5)} + T_{nm}^{(6)}) \\ &\times \delta(S_m + S_n)\}|A_m|^2 A_n, \end{aligned} \tag{21}$$

which is the sum of (16$a$) and (16$b$) after the identity in (20) is used. The system (21) together with

$$\sum_{m=-N}^{N} |A_m|^2 = 1, \tag{22}$$

which is derived from (11), consists of $(2N+1)$ equations for $(2N+1)$ unknowns $R_{20}$ and $A_n (n = -N, \ldots, -1, 1, \ldots, N)$.

The semi-regular solutions of (21) and (22) are

$$|A_1|^2 = \cdots = |A_N|^2 = 1/(2N), \quad 4R_{20}^{(s)} = \frac{1}{2N}\sum_{m=1}^{N}(T_{1m}^{(s)} + T_{1,-m}^{(s)}), \tag{23a}$$

where

$$T^{(s)}_{nm} = (T^{(1)}_{nm} + T^{(1)}_{-n,m} + T^{(3)}_{nm} + T^{(3)}_{-n,m} + T^{(7)}_{nm} + T^{(7)}_{-n,m} + T^{(8)}_{nm} + T^{(8)}_{-n,m}) + (T^{(2)}_{nm} + T^{(4)}_{-n,m} + T^{(5)}_{nm} + T^{(6)}_{-n,m})\delta(S_m - S_n) + (T^{(2)}_{-n,m} + T^{(4)}_{nm} + T^{(5)}_{-n,m} + T^{(6)}_{nm}) \times \delta(S_m + S_n). \tag{23b}$$

The simplest form of such solutions corresponds to the case of standing rolls, where

$$N = 1, \quad R_{20} = (1/8)(T^{(s)}_{11} + T^{(s)}_{1,-1}), \quad |A_1|^2 = 1/2. \tag{24}$$

## 4. Stability analysis

The analysis of the finite-amplitude oscillatory convection presented in the previous section has shown that an infinite manifold of solutions could exist even though this manifold represents only an infinitesimal fraction of the manifold of the solutions (9*a*)–(9*c*) of the linear problem. To distinguish the physically realizable solution from among all possible oscillatory solutions, the stability of $V, \theta, \phi$ with respect to arbitrary three-dimensional disturbances $V_d$, $\theta_d$, $\phi_d$ must be investigated. The time-dependent disturbances can be assumed to be in the form

$$(V_d, \theta_d, \phi_d) = [V'(x, y, z, t), \theta'(x, y, z, t), \phi'(x, y, z, t)] \exp(\sigma t), \tag{25}$$

where $\sigma$ is the growth rate of the disturbances. When the governing equations and the boundary conditions of the form (7*a*)–(7*e*) for the finite-amplitude oscillatory flow are subtracted from the corresponding equations and boundary conditions for the total dependent variables for the oscillatory flow and the disturbance quantities, and the resulting system is linearized with respect to the disturbance quantities, we obtain the following stability system:

$$\nabla^2 \left[\varepsilon\phi'\left(\frac{\mathrm{d}}{\mathrm{d}\tilde{\phi}}\right) K(\phi_\mathrm{B} + \varepsilon\phi)\Delta_2 V + K(\phi_\mathrm{B} + \varepsilon\phi)\Delta_2 V'\right] + \left(\frac{\partial}{\partial z}\right) \times \left\{\varepsilon \boldsymbol{\Omega} V \cdot \nabla \left[\phi'\left(\frac{\mathrm{d}}{\mathrm{d}\tilde{\phi}}\right) K(\phi_B + \varepsilon\phi)\right] + \boldsymbol{\Omega} V' \cdot \nabla K(\phi_B + \varepsilon\phi)\right\} - R\Delta_2\theta' = 0, \tag{26a}$$

$$\left(\frac{\partial}{\partial t} + \sigma - \frac{\delta\partial}{\partial z}\right)\left(-\theta' + \frac{S\phi'}{\delta}\right) + R\left(\frac{\mathrm{d}\theta_B}{\mathrm{d}z}\right)\Delta_2 V' + \nabla^2\theta' = \varepsilon R(\boldsymbol{\Omega} V \cdot \nabla\theta' + \boldsymbol{\Omega} V' \cdot \nabla\theta), \tag{26b}$$

$$\left(\frac{\partial}{\partial t} + \sigma - \frac{\delta\partial}{\partial z}\right)\left[(-1 + \phi_B)\theta' + \theta_B\phi' + \varepsilon\phi\theta' + \varepsilon\phi'\theta - \frac{C\phi'}{\delta}\right] + R\left(\frac{\mathrm{d}\theta_B}{\mathrm{d}z}\right)\Delta_2 V' = \varepsilon R(\boldsymbol{\Omega} V \cdot \nabla\theta' + \boldsymbol{\Omega} V' \cdot \nabla\theta), \tag{26c}$$

$$V' = \theta' = 0 \quad \text{at} \quad z = 0, \tag{26d}$$

$$V' = \theta' = \phi' = 0 \quad \text{at} \quad z = 1. \tag{26e}$$

When expansion (8) is used in (26*a*)–(26*e*) it becomes evident that the stability system

can be solved by a similar expansion

$$(V',\theta',\phi',\sigma) = [(V'_{00}+\delta V'_{01}+\cdots),(\theta'_{00}+\delta\theta'_{01}+\cdots),(\phi'_{00}+\delta\phi'_{01}+\cdots),$$
$$(\sigma_{00}+\delta\sigma_{01}+\cdots)] + \varepsilon[(V'_{10}+\delta V'_{11}+\cdots),(\theta'_{10}+\delta\theta'_{11}+\cdots),$$
$$(\phi'_{10}+\delta\phi'_{11}+\cdots),(\sigma_{10}+\delta\sigma_{11}+\cdots)] + \varepsilon^2[(V'_{20}+\delta V'_{21}+\cdots),$$
$$(\theta'_{20}+\delta\theta'_{21}+\cdots),(\phi'_{2(-1)}/\delta+\phi'_{20}+\delta\phi'_{21}+\cdots),(\sigma_{20}+\delta\sigma_{21}+\cdots)]+\cdots, \quad (27)$$

where the expansion for $\phi'$ is singular at order $\varepsilon^2$ as $\delta\to 0$, but it turns out that the $O(1/\delta)$ term is needed in the stability analysis since the $O(\varepsilon^2)$ stability problem is found to be forced by a term of order $1/\delta$ in the solute equation for the disturbances.

We also restrict ourselves to those disturbances whose dependent variables $V'$, $\theta'$, $\phi'$ have wavenumbers $a'=a_c$ and frequencies $\omega'=\omega_c$. Then the most critical disturbances, which have the maximum growth rate, are found to be characterized by $\sigma_0=0$, where

$$\sigma_0=\sigma_{00}+\delta\sigma_{01}+\cdots.$$

The linear solutions for the dependent variables of the disturbances at order $\delta^0$ are found to be of the form (9*a*)–(9*c*), provided $A_n^{\pm}$ and $N$ are replaced by arbitrary constants $\tilde{A}_n^{\pm}$ and $\infty$, respectively.

In analogy to the solvability conditions for the oscillatory motion presented in the previous section, the solvability conditions for the disturbance systems at order $\varepsilon^n$ $(n\geqslant 1)$ require us to define two independent particular solutions of the linear system for the disturbances. These solutions, designated either by $\tilde{V}_{00n}^{\pm}$ and $\tilde{\theta}_{00n}^{\pm}$ or by $\tilde{V}_{00n}$ and $\tilde{\theta}_{00n}$, have the same form as either (14) or (20), provided that the $A_n^{\pm}$ are replaced by $\tilde{A}_n^{\pm}$. The solvability conditions for the disturbance system at order $\varepsilon$ are derived similarly to the corresponding ones for the oscillatory flow system. Similarly to the result for $R_{10}$ presented in the previous section, we found that the expression for $\sigma_{10}$ obtained from these solvability conditions consisted of sum of terms involving integrals of the form $\langle\eta_n^{\pm}\eta_l^{\pm}\eta_p^{\pm}\rangle$, which are all zero again due to the time averaging, and so $\sigma_{10}=0$. Application of this procedure to disturbance systems at orders $\varepsilon\delta^m(m\geqslant 1)$ then implies that $\sigma_{1m}=0$. The solution to the order $\varepsilon$ of the disturbances is given by (B1) in the Appendix B.

At order $\varepsilon^2/\delta$ the system (26) yields

$$\left(\frac{\partial}{\partial t_1}-\frac{\partial}{\partial z}\right)\phi'_{2(-1)}=-\sigma_{20}\phi'_{00}, \quad (28a)$$

$$\phi'_{2(-1)}=0 \quad \text{at} \quad z=1, \quad (28b)$$

where $t_1$ is defined in (A1) (Appendix A).

The solution to (28*a*) and (28*b*) is of the form

$$\phi'_{2(-1)}=\sum_{n=-\infty}^{\infty}[\tilde{f}_n(z)\tilde{A}_n^{+}\eta_n^{+}+\tilde{f}_n^{*}(z)\tilde{A}_n^{-}\eta_n^{-}]\sigma_{20}, \quad (29a)$$

where

$$\tilde{f}_n(z)=\left(\frac{2\pi^2}{[CG(\pi^2-\omega_{01}^2)^2]}\right)\{-(\pi^2+\omega_{01}^2)\sin(\pi z)+2i\pi\omega_{01}S_n[\cos(\pi z)$$
$$+\exp(i\omega_{01}S_n z-i\omega_{01}S_n)]+\pi\pi^2-\omega_{01}^2)(1-z)\exp[i\omega_{01}S_n(z-1)]\}. \quad (29b)$$

At order $\varepsilon^2$ the system (26*a*)–(26*e*) can be reduced to the form given by (B 2) in

the appendix B. Solvability conditions for the system (B 2) yield a set of equations involving $\sigma_{20}$ which is given by (B 3*a*).

*Standing waves*

Using (16) in (B 3*a*) and considering first standing wave disturbances acting on the standing waves, we find

$$2S_0\sigma_{20}\tilde{A}_n + A_n \sum_{m=-N}^{N} \tilde{T}^{(s)}_{nm} A^*_m \tilde{A}_m = 0, \tag{30a}$$

where

$$\tilde{A}_n \equiv \tilde{A}^+_n + \tilde{A}^-_n, \quad \tilde{T}^{(s)}_{nm} = T^{(s)}_{nm} + T^{(s)}_{n,-m}. \tag{30b}$$

Using (23*b*) and (A 4) in (30*a*), we find that the matrix $\tilde{T}^{(s)}_{nm}$ has the following symmetries:

$$\tilde{T}^{(s)}_{nm} = \tilde{T}^{(s)}_{mn} = \tilde{T}^{(s)}_{n,-m} = \tilde{T}^{(s)}_{-n,m}, \tag{31a}$$

$$\tilde{T}^{(s)}_{nn} = \tilde{T}^{(s)}_{11} \quad (n = -N, \ldots, -1, 1, \ldots, N). \tag{31b}$$

Using (31) and following either Schluter, Lortz & Busse (1965) or Busse & Riahi (1980), we find that $N$ eigenvalues $\sigma_{20}$ of (30) are zero and the rest of the eigenvalues are real and satisfy the characteristic equation

$$\det |2S_0\sigma_{20}\delta_{nm} + \tilde{T}_{nm} A_{-m} A_n| = 0 \quad (n, m = 1, \ldots, N), \tag{32a}$$

where

$$\delta_{nm} = 1 \quad \text{for} \quad n = m \quad \text{and} \quad 0 \quad \text{for} \quad n \neq m. \tag{32b}$$

Equation (32*a*) is a polynomial equation in $\sigma_{20}$ of degree $N$ of the form

$$\sum_{n=0}^{N} b_n \sigma^n_{20} = 0, \tag{33a}$$

where

$$b_N = (2S_0)^N, \tag{33b}$$

$$b_{N-1} = \sum_{m=1}^{N} \tilde{T}^{(s)}_{nn} |A_n|^2, \tag{33c}$$

$$b_{N-2} = \sum_{n,m=1(m>n)}^{N} (\tilde{T}^{(s)}_{nn} \tilde{T}^{(s)}_{mm} - \tilde{T}^{(s)}_{nm} \tilde{T}^{(s)}_{mn}) |A_n A_m|^2. \tag{33d}$$

Our calculation of $S_0$ for various values of $G$ and $G_t$, which is presented in Appendix B, indicates that $S_0$ is positive. Hence $b_N$ is positive. Using (20*a*) and (B 3*b*), we find that

$$b_{N-1} = 4R_{20} \tag{34}$$

for rolls. As the results in the § 5 indicate, the value of $R_{20}$ for standing rolls is positive. Hence $b_{N-1}$ is positive. Since all the roots of (33*a*) are real and the coefficients $b_N$ and $b_{N-1}$ are both positive, we conclude from the sign rule of Descarts for polynomials that at least one root of (33*a*) is positive, provided that the coefficient $b_{N-2}$, given by (40*d*), is negative. Hence a three-dimensional standing wave is unstable if

$$b_{N-2} < 0. \tag{35}$$

The inequality (35) clearly holds if

$$\tilde{T}^{(s)}_{nm} > \tilde{T}^{(s)}_{nn} > 0 \quad (m > n). \tag{36}$$

For two-dimensional flow in the form of standing rolls ($N = 1$), (32) yield

$$2S_0\sigma_{20} = -4R_{20}. \tag{37}$$

Hence $\sigma_{20} < 0$ and standing rolls are stable.

*Simple travelling waves*

Considering left-(right-) travelling wave disturbances acting on the finite-amplitude motion in the form of left-(right-) travelling waves, we find that the results (30)–(37) can be applicable for such motion, provided $A_n$, $\tilde{A}_n$, $2S_0$ and $\tilde{T}^{(s)}_{nm}$ are replaced, respectively, by $A^+_n(A^-_n)$, $\tilde{A}^+_n(\tilde{A}^-_n)$, $S_0$ and $\tilde{T}^{(st)}_{nm}$, where

$$\tilde{T}^{(st)}_{nm} = T^{(st)}_{nm} + T^{(st)}_{n,-m}. \tag{38}$$

*General travelling waves*

Considering general travelling wave disturbances acting on the oscillatory motion in the form of the general travelling waves already introduced, we find that the results (30)–(37) are applicable for such motion, provided $A_n$, $\tilde{A}_n$ and $\tilde{T}^{(s)}_{nm}$ are replaced, respectively, by $[(0.5-b)/N]^{0.5}$, $\tilde{A}^+_n$ and $\tilde{T}^{(gt)}_{nm}$, where

$$\tilde{T}^{(gt)}_{nm} = T^{(gt)}_{nm} + T^{(gt)}_{n,-m}, \tag{39a}$$

$$\begin{aligned} T^{(gt)}_{nm} = {} & (T^{(1)}_{nm} + T^{(1)}_{-n,m}) + (T^{(2)}_{nm} + T^{(4)}_{-n,m}) \left[\frac{0.5+b}{0.5-b}\right] \delta(S_m - S_n) + (T^{(2)}_{-n,m} + T^{(4)}_{nm}) \\ & \times \left[\frac{0.5+b}{0.5-b}\right] \delta(S_m + S_n) + (T^{(3)}_{nm} + T^{(3)}_{-n,m}) \left[\frac{0.5+b}{0.5-b}\right] + (T^{(5)}_{nm} + T^{(6)}_{-n,m}) \\ & \times \left[\frac{0.5+b}{0.5-b}\right]^{0.5} \delta(S_m - S_n) + (T^{(5)}_{-n,m} + T^{(6)}_{nm}) \left[\frac{0.5+b}{0.5-b}\right]^{0.5} \delta(S_m + S_n) \\ & + (T^{(7)}_{nm} + T^{(7)}_{-n,m}) \left[\frac{0.5+b}{0.5-b}\right]^{1.5} + (T^{(8)}_{nm} + T^{(8)}_{-n,m}) \left[\frac{0.5+b}{0.5-b}\right]^{0.5}. \end{aligned} \tag{39b}$$

*Inclined disturbances*

So far the analysis has been restricted to disturbances whose wavenumber vectors coincide with those of the oscillatory motion. We now consider the stability of the oscillatory motion with respect to disturbances in the form of rolls whose wave number vectors are inclined with respect to any wavenumber vector of the oscillatory motion. The horizontal dependence of $V'_{00}$ and $\theta'_{00}$ for such disturbances can be written as

$$\sum_{r=-1}^{1} \tilde{A}^+_r \tilde{\eta}^+_r + \tilde{A}^-_r \eta^-_r, \quad \tilde{\eta}^{\pm}_r \equiv \exp(\mathrm{i}\tilde{\boldsymbol{a}}_r \cdot \boldsymbol{r} \pm \mathrm{i}\omega_{01} t_1). \tag{40}$$

Here the wavenumber vector $\tilde{\boldsymbol{a}}_r$ of such disturbances satisfies properties of the form (10). For such disturbances, solvability conditions for (B 2) in Appendix B can be simplified to those given by (B 4).

The growth rate $\sigma_{20}$, given by (B 4), for inclined disturbances in the form of either standing rolls or travelling rolls, acting on the finite-amplitude oscillatory motion, can

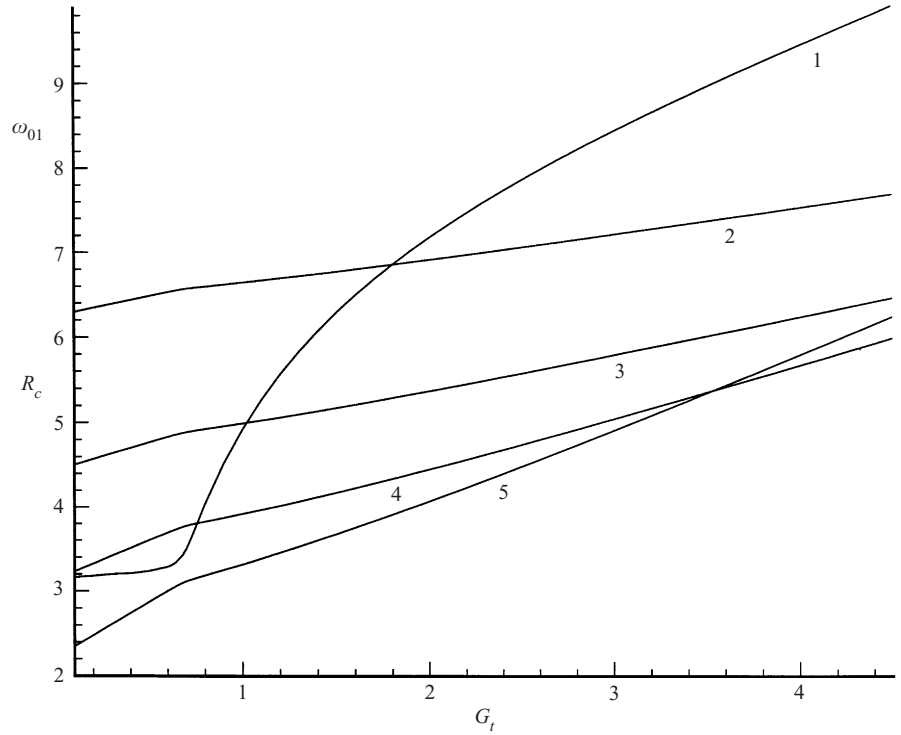


FIGURE 1. The frequency $\omega_{01}$ and the critical value of the scaled Rayleigh number $R_C$ versus $G_t$. A number just below a curve labels the curve. Curve 1 shows $\omega_{01}$. Curves 2, 3, 4 and 5 shows $R_C$ and correspond respectively, to $G = 1.01$, 2.0, 4.0 and 8.0.

then be determined for various values of the angle of the inclination between $\tilde{\boldsymbol{a}}_r$ and the wavenumber vectors $\boldsymbol{a}_n$ of the oscillatory motion.

## 5. Results and discussion

### 5.1. *Linear problem*

The linear system and its eigenvalue problem, which led to the results (9)–(14), are, in general, functions of the two parameters $G$ and $G_t$. These two parameters are related to the scaled Stefan number $S$ and the scaled compositional ratio $C$ as given in (4$a$) and (13$c$). Given $S$ and $C$, $G$ and $G_t$ can be determined uniquely and vice versa. The results provided in this paper are given as functions of $G$ and $G_t$ since these parameters are found to be particularly relevant for the oscillatory system as was also noted earlier by Anderson & Worster (1996) for their linear system. The results for the frequency $\omega_{01}$ of the oscillatory motion and for $R_C$, given by

$$R_C = R_{00c} + \delta R_{01} + O(\delta^2), \tag{41}$$

as functions of $G_t$ and for given values of $G$ are presented in figure 1. Since $\omega_{01}$ was found to be rather insensitive to $G$, at least in the range $1.01 \leqslant G \leqslant 8.0$, its values as function of $G_t$ are presented in the figure 1 for a given value of $G$ in this range. Here, and thereafter, the value of $\delta = 0.2$ is chosen to evaluate $R_C$ and other quantities whose values may depend on $\delta$. It is seen from the results presented in this figure that $\omega_{01}$ increases with $G_t$ and has a rather high rate of increase with respect to

$G_t$ in the range $0.7 \leqslant G_t \leqslant 1.0$. $R_C$ generally increases with $G_t$ and increases with decreasing $G$. Since $S$ represents a measure of the latent heat relative to the heat content and $C$ represents the difference between the characteristic compositions of the solid and liquid phases and the compositional variation of the liquid, the linear system is destabilized as $S$ increases, for a given $C$, or as $C$ decreases, for a given $S$. Hence, the linear system is destabilized as $G$ increases. To uncover some non-trivial effects of the competing parameters $S$ and $C$, or $G_t$ and $G$, on the linear flow system, we make the following observations based on the results presented in figure 1. Since $G_t$ increases with decreasing $C$, for a given $G$, then $S$ has to decrease by the same rate as $C$ in order to maintain the value of $G$. It is also seen from the figure 1 that $R_C$ increases with $G_t$ for a given $G$, so that the linear system is stabilizing as $G_t$ increases for a given G. Hence, the Stefan number is more effective than the compositional ratio $C$ in stabilizing the flow as $G_t$ increases. For a given $G_t$, $R_C$ generally decreases with increasing $G$, provided $G_t$ is not too large. Since $S$ increases with $G$ and $C$ decreases with increasing $G$ for $G > 2.0$, then the destabilizing effect on the linear system is understandable and again implies that the Stefan number is more effective than the compositional ratio. It can also be seen from the results presented in figure 1 that the parameter $G_t$ appears to be, in a sense, more effective than $G$ since for sufficiently large $G_t$, the flow at a larger $G$ can be more stable than the one at a relatively smaller $G$.

### 5.2. *Nonlinear problem*

An important quantity due to the nonlinear effects is the coefficient $R_{20}$. As can be seen from the expansion (8), $R_{20}$ represents a contribution to the change in $R$ required to obtain given finite amplitude $\varepsilon$ for a nonlinear solution. As shown in § 3, there is no term linear in $\varepsilon$ in the expansion for $R$, and, thus, the amplitude of the convection is of order

$$\varepsilon = \pm[(R - R_c)/R_{20}]^{1/2}. \tag{42}$$

The sign of $R_{20}$ determines whether the oscillatory solution exists for values of $R$ above or below $R_c$. For supercritical convection, where $R > R_c$, the amplitude of convection is largest, provided the value of $R_{20}$ is smallest among all the solutions to the nonlinear problem. In the present problem $R_{20}$ is due to both nonlinear convective terms in the temperature equation given in (A 3) and the nonlinear interactions between the flow velocity and the non-uniform and nonlinear permeability associated with the perturbation to the basic-state solid fraction.

The coefficients $R_{20}$, given by (21*a*) and (23*a*) for the standing rolls and simple travelling rolls, respectively, were computed for various values of $G$, $G_t$ and $K_2$. It was found that $R_{20}$ is positive, and, thus, these oscillatory rolls are supercritical. Some typical results are presented in figure 2 for $R_{20}$ versus $G_t$ and for two different values of $G$ and $K_2$ in the case of rolls. Since the preferred mode is anticipated to have the smallest value for $R_{20}$ among all the possible modes, then the results presented in the figure 2 indicate that simple travelling rolls are probably preferred over the standing rolls in most of the range of values for the parameters $G$, $G_t$ and $K_2$, except in a narrow and relatively small range of values for $G_t$ where standing rolls are probably preferred over the simple travelling rolls. Our stability results, to be presented in the next subsection, confirm these anticipations. It is seen that both simple travelling and standing modes are stabilized as $G_t$ increases. Typical results on the variation of $R_{20}$ with respect to $G$, $G_t$ and $K_2$ are presented in figures 3 and 4. Figure 3 presents $R_{20}$ versus $G_t$ for simple travelling rolls and $K_2 = 0.15$ and for $G = 2.0$, 4.0 and 8.0. It is

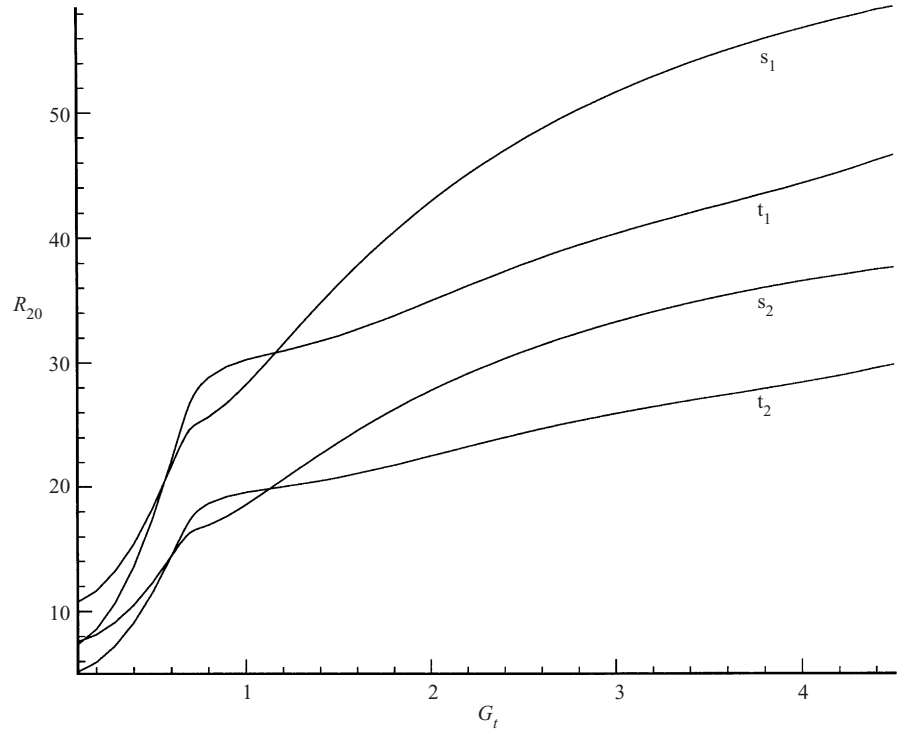


FIGURE 2. $R_{20}$ versus $G_t$ for rolls. $R_{20}$ for standing rolls ($s$) and simple travelling rolls ($t$) are plotted for $G = 2.0$ and $K_2 = 0.05$ ($s_1, t_1$), and for $G = 4.0$ and $K_2 = 0.1$ ($s_2, t_2$).

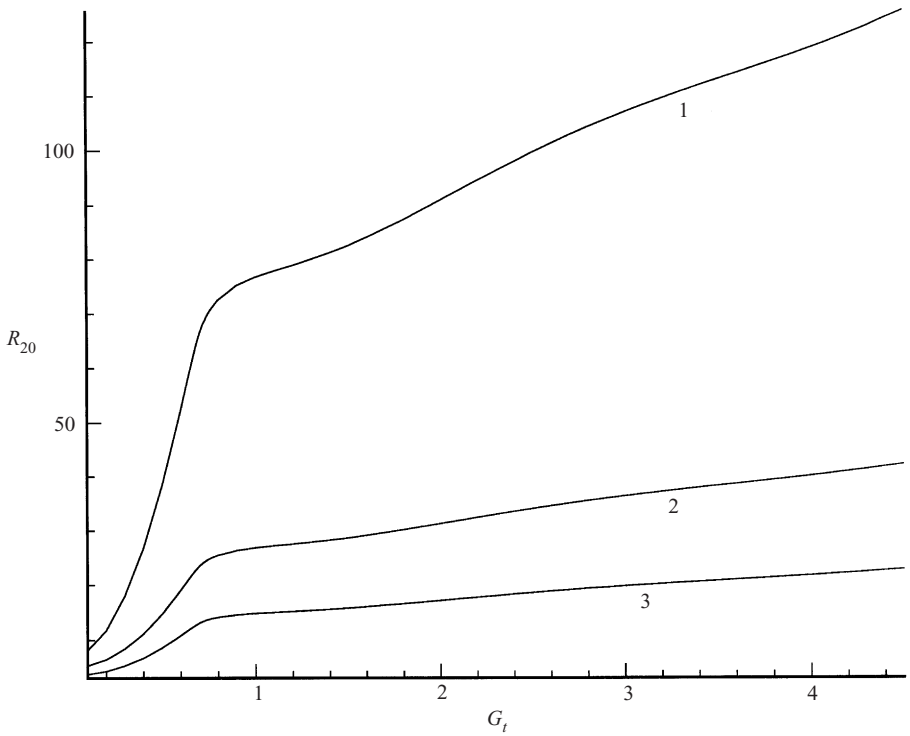


FIGURE 3. $R_{20}$ versus $G_t$ for simple travelling rolls. $K_2 = 0.15$, and graphs labelled 1, 2 and 3 present, respectively, $R_{20}^{(st)}$ for $G = 2.0$, 4.0 and 8.0.

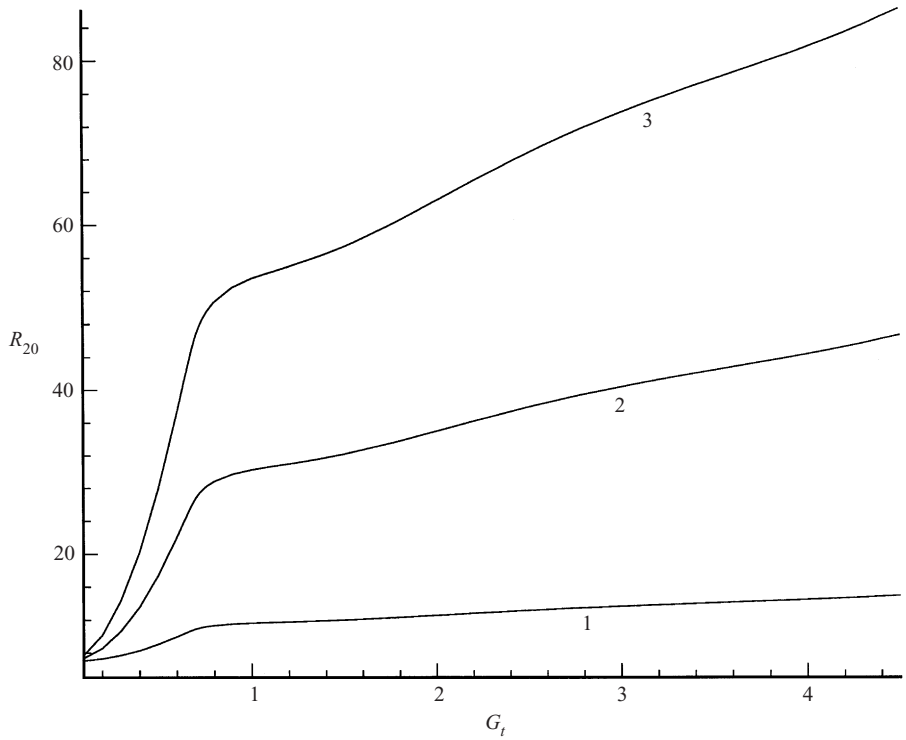


FIGURE 4. $R_{20}$ versus $G_t$ for simple travelling rolls. $G = 2.0$, and graphs labelled 1, 2 and 3 present, respectively, $R_{20}^{(st)}$ for $K_2 = 0.01$, 0.05 and 0.10.

seen from this figure that the simple travelling mode is stabilized with increasing $G$. Our other data indicated that the same qualitative result also holds for the standing rolls. Figure 4 presents $R_{20}$ versus $G_t$ in the case of simple travelling rolls for $G = 2.0$ and $K_2 = 0.01$, 0.05 and 0.10. It is seen from this figure that the simple travelling mode is stabilized with increasing $K_2 (K_2 > 0)$ and the rate of stabilization of the mode with respect to $G_t$ decreases with decreasing $K_2$. Our other data indicated that the same qualitative result also holds for the standing rolls. The result in the limit of $K_2 = 0$ is not shown in these figures, but it was found that the simple travelling and standing rolls are independent of $G_t$ and are destabilized with increasing $G$ in the limit of zero $K_2$.

The nonlinear results presented in the previous paragraph are consistent with the physical properties of the parameters $G$, $G_t$ and $K_2$. As discussed in the previous subsection and generally in agreement with the linear results, increasing $G$ is destabilizing, while increasing $G_t$ is generally stabilizing. Hence, $R_{20}$ generally decreases with either increasing $G$ or decreasing $G_t$. For the oscillatory modes, it should be noted that $K_2$ represents a leading-order effect of the inverse of the permeability of the mushy layer in the present problem. It is associated with the curvature in the $K(\tilde{\phi})$ relation and is usually positive. The permeability decreases with increasing $K_2$. Thus, the flow is stabilized as $K_2$ increases and destabilized as $K_2$ decreases. Hence, $R_{20}$ increases with $K_2$.

It should be noted that since the solute flux, or equivalently here the heat flux $H = \langle \tilde{\theta} \tilde{\boldsymbol{u}} \cdot \boldsymbol{z} \rangle$, is proportional to square of $\varepsilon$ given by (42), to the leading-order, then $H$ is inversely proportional to $R_{20}$, and the flow solution with the smallest value of $R_{20}$

transports the maximum amount of heat or solute to the leading-order. In addition, in direct analogy to the case of stationary thermal convection in planar layers (Busse 1967), one can expect that the preferred nonlinear oscillatory solutions, in the limit of small $\varepsilon$, correspond to those that represent the smallest value of $R_{20}$, in the limit of small $\delta$, among all the solutions admitted by the solvability conditions (16$a$).

Using (17) and (23), the coefficients $R_{20}^{(st)}$ and $R_{20}^{(s)}$ for oscillatory squares ($N = 2$) and oscillatory hexagons ($N = 3$) were computed for various values of $G$, $G_t$ and $K_2$. As in the case of rolls, it was found that $R_{20}^{(st)}$ and $R_{20}^{(s)}$ are positive for squares and hexagons, with either upward flow at the cell centres (up-hexagons) or downward flow at the cell centres (down-hexagons), and their values for $R_{20}$ are generally larger than the corresponding values for the oscillatory rolls. Thus, similarly to the case of oscillatory rolls, it was found that the three-dimensional simple travelling wave and standing wave solutions in the forms of squares and hexagons are supercritical. Although no rigorous proof has been found, it is likely that the above results for $N < 4$ are also generally applicable to the $N \geqslant 4$ cases.

The coefficient $R_{20}^{(gt)}$, given by (19$a$), for the semi-regular solutions in the form of general travelling waves indicates that $R_{20}^{(gt)}$ is symmetric with respect to $b = 0$, where $b = 0$ corresponds to the case of standing waves. This result implies that, for a given $|b|$ in the range (19$b$), there are always two sets of general travelling waves with equal stability properties. In addition, it is found from (19$a$) that

$$R_{20}^{(gt)} > R_{20}^{(st)} \quad \text{for} \quad R_{20}^{(s)} > R_{20}^{(st)}, \tag{43a}$$

$$R_{20}^{(gt)} > R_{20}^{(s)} \quad \text{for} \quad R_{20}^{(st)} > R_{20}^{(s)}, \tag{43b}$$

$$R_{20}^{(gt)} = R_{20}^{(s)} \quad \text{for} \quad R_{20}^{(st)} = R_{20}^{(s)}. \tag{43c}$$

Hence, all the general travelling waves in the range (19$b$) for $b$ are supercritical. In addition, the results (43$a$)–(43$c$) imply that general travelling waves are not expected to be preferred, in general, due to (43$a$) and (43$b$), unless (43$c$) holds at some singular values in the parameter space where mixed modes consisting of general travelling waves, standing waves and simple travelling waves can all coexist.

We also examined the vertical distribution of the solid fraction at different locations in the horizontal direction and in time for the solutions in the form of oscillatory rolls parallel to the $x$-axis. Some typical results are presented in figures 5 and 6 for the vertical distribution of the solid fraction in the cases of standing and simple travelling rolls, respectively. For these figures $\delta = 0.2$, $G = 2.0$, $K_2 = 0$, and $\varepsilon = 0.002$ is chosen, which is the maximum value of $\varepsilon$ beyond which the solid fraction becomes negative. This is based on the physical grounds that deviation of the total solid fraction $\tilde{\phi}$ from $\phi_B$ due to convection cannot make $\tilde{\phi}$ negative. We have chosen a zero value for $K_2$ in these figures since $\tilde{\phi}$ is found to be almost insensitive to $K_2$ at such a small value of $\varepsilon$. Figure 5 presents results for the standing rolls at $G_t = 0.7$. It can be seen from this figure that the solid fraction at $t = 0$ along the boundary between two rolls ($y = 0$) decreases due to the convection in most of the layer, and $(\phi_B - \tilde{\phi})$ is largest and positive at some interior point in the mushy layer away from the boundaries, which implies that chimneys may be initiated at some location within the mushy layer. This result is in agreement with numerical observations by Schulze & Worster (1999) in a two-layer model for a two-dimensional steady system. However, the solid fraction at a later time ($t = 0.5$) along the same boundary appears to be reduced by the convection mostly near the lower boundary implying the possibility of chimney formation near the lower boundary of the mushy zone at such a later time. We also found that the

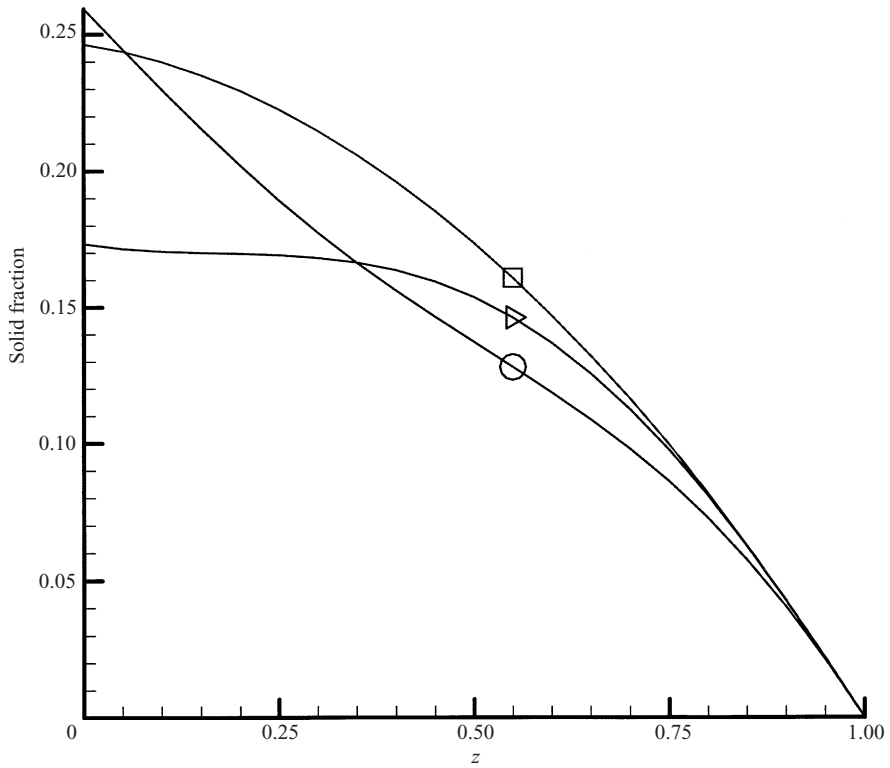


FIGURE 5. Solid fraction for standing rolls versus $z$ for $G = 2.0$, $K_2 = 0$ and $G_t = 0.7$. Here graphs labelled by the square, circle and triangle symbols show, respectively, the basic solid fraction $\phi_B$, $\tilde{\phi}(y = 0, z, t = 0)$ and $\tilde{\phi}(y = 0, z, t = 0.5)$.

solid fraction at both $t = 0$ and 0.5 along the centreline line ($y = 0.5$) is close to the basic solid fraction $\phi_B$ throughout the depth of the mushy layer, which implies that it is unlikely that chimneys can be initiated along the centreline at these two instants in time. Figure 6 presents results for the right-travelling rolls at $G_t = 0.1$. It can be seen from this figure that the solid fraction at $t = 0$ along the centreline ($y = 0.5$) increases due to the convection and its maximum value occurs at some region near the lower boundary, while the solid fraction at a later time ($t = 0.5$) along the centreline decreases due to the convection mainly away from the upper boundary. We also found that the solid fraction at $t = 0$ along the boundary between two rolls was close to that along the centreline at $t = 0.5$ throughout the depth of the layer. Additional calculated data indicated similar features regarding chimney initiation in most of the layer in the case of convection in the form of left-travelling rolls. A common feature of these results is that chimneys may be initiated at some location within the layer or near the lower boundary but probably not near the upper boundary of the layer.

To discuss the physical interpretation of the results on the solid fraction distribution described in the previous paragraph, it is appropriate to describe briefly first the results determined by Anderson & Worster (1996) on the structure of a travelling mode in the linear regime, which were in agreement with our calculated data for the travelling rolls. In contrast to the steady-state case, where the perturbations to the solid fraction lead to vertical chimneys of reduced solid fraction and vertically oriented compositional stripes, due to the variation in the solid fraction at the lower boundary (Anderson

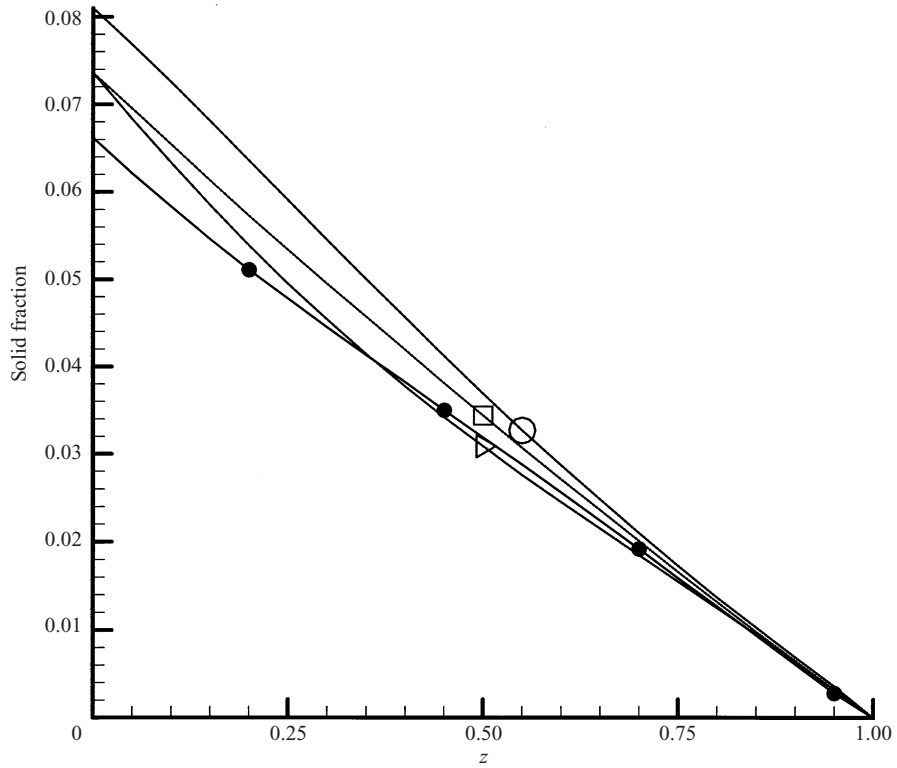


FIGURE 6. Solid fraction for simple travelling rolls versus $z$ for $G = 2.0$, $K_2 = 0$ and $G_t = 0.1$. Here graphs labelled by the square, circle, triangle and filled circle symbols show, respectively, $\phi_B$, $\tilde{\phi}(y = 0.5, z, t = 0)$, $\tilde{\phi}(y = 0.5, z, t = 0.5)$ and $\tilde{\phi}(y = 0, z, t = 0.5)$.

& Worster 1995), the chimneys and the compositional strips in a travelling wave state can be inclined. The non-vertical directions are due to the non-zero values of the phase speed of such a wave relative to the uniform upward speed of the mushy layer, and, consequently, the chimneys develop variable slopes relative to the vertical direction. Furthermore, the chimneys away from the boundaries are mostly within a roll, rather than between two convection rolls as in the steady-state case. These main differences in the orientations of the chimneys and the compositional strips in the steady-state and the oscillatory-state cases are due to the fact that the solid-fraction perturbation is out of phase with the thermal and flow fields in the oscillatory case, while the solid-fraction perturbation is in phase with the flow and thermal fields in the steady case. In the present nonlinear oscillatory problem, the non-vertical features of the chimneys and the compositional strips still persist in the parameter regime where the simple travelling rolls are stable. In the parameter regime where the standing rolls are stable, the chimneys and the compositional strips are in the vertical direction since the phase speed of these rolls is zero, but the vertical extent of the chimneys may vary depending on the variation of the solid-fraction perturbation with respect to time.

### 5.3. *Stability problem*

Condition (35) has been computed numerically for different integers $N$ and various values of $\psi_{nm}(|\psi_{nm}| \leqslant 1)$. In all cases of $N > 1$ and $\psi_{nm}$ that have been investigated

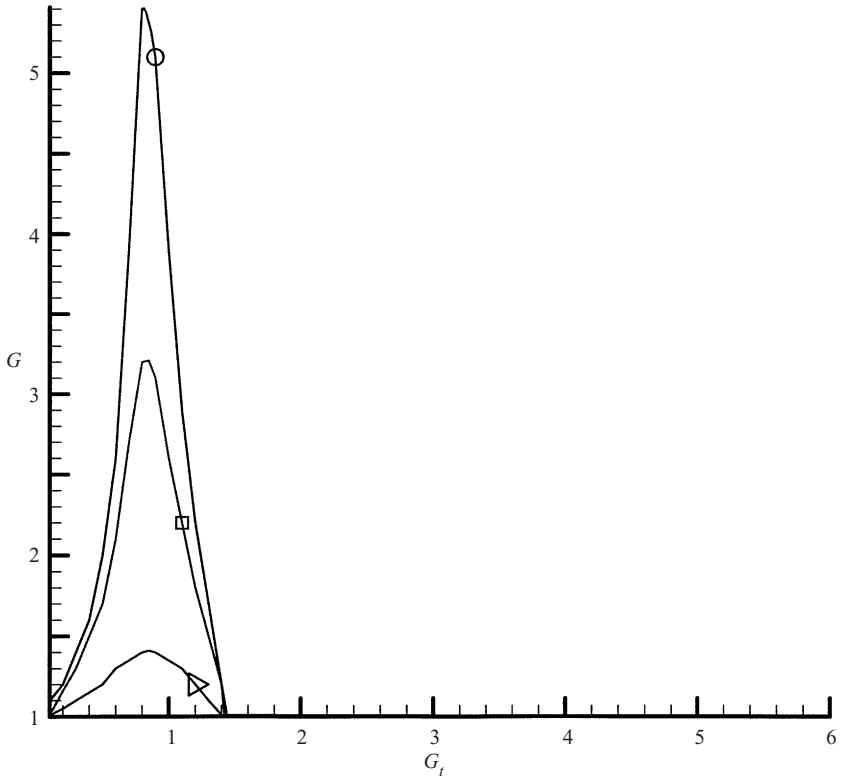


FIGURE 7. Regions of stable and preferred oscillatory modes of convection in the $(G_t, G)$-plane for different values of $K_2$. The stability boundaries labelled by the circle, square and triangle symbols correspond respectively, to $K_2 = 0.07$, 0.05 and 0.01. For a given $K_2$, standing rolls are stable in the small region bounded by the stability curve, while simple travelling rolls are stable outside that region.

condition (35) was found to be valid for three-dimensional oscillatory solutions in the form of standing waves, general travelling waves and simple travelling waves. Hence, all the three-dimensional solutions of such forms are unstable. Using (B 4), the growth rates for the inclined disturbances, acting on the two-dimensional oscillatory solutions, are computed at various values of $\Psi_{r1}$. Disturbances in the form of standing waves, general travelling waves and simple travelling waves acting on the oscillatory flow in the form of standing rolls, general travelling rolls and simple travelling rolls were studied. The results of such studies and computation indicated that, depending on the parameter values for $G$, $G_t$ and $K_2$, only oscillatory rolls in the form of either simple travelling rolls or standing rolls, which correspond to the smallest associated $R_{20}$ coefficient, are stable with respect to such disturbances. Hence, among all the two- and three-dimensional oscillatory solutions to the nonlinear problem, only simple travelling rolls or standing rolls are stable and, thus, preferred depending on the range of values for $G$, $G_t$ and $K_2$.

Figure 7 presents stability regions of the preferred solutions in the $(G_t, G)$-plane for different values of $K_2$. The stability boundaries for the cases of $K_2 = 0.07$, 0.05 and 0.01 are shown by a circle, a square and a triangle, respectively. These stability boundaries are all closed curves and their lower parts lie on the $G_t$-axis. Standing rolls are stable in a rather small region, designated here by $D(K_2)$, which is bounded

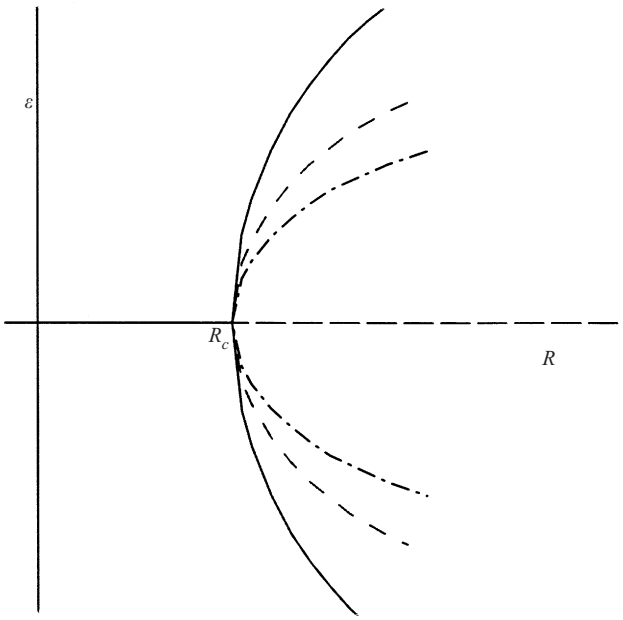


FIGURE 8. Bifurcation diagram in the $(R, \varepsilon)$-plane. Here solid lines are stable branches, while dashed and dashed-dot lines are unstable branches. The dashed-dot curve corresponds to general travelling rolls. The solid curve corresponds to the stable standing (simple travelling) rolls inside (outside) the small region $D(K_2)$, while the dashed curve corresponds to the unstable standing (simple travelling) rolls outside (inside) $D(K_2)$.

by the stability curve, for a given $K_2$, while simple travelling rolls are stable outside the region $D(K_2)$. The stability region $D(K_2)$ for the standing rolls shrinks to zero in the limit of $K_2 = 0$, and simple travelling rolls become the only stable flow pattern in this case. Thus, the region in the $(G_t, G)$-plane for the stable (unstable) simple travelling rolls (or unstable (stable) standing rolls) decreases (increases) with increasing $K_2$. These results are consistent with the destabilizing effect of larger permeability on the standing rolls. Figure 8 presents a qualitative bifurcation diagram for the oscillatory rolls in the $(R, \varepsilon)$-plane. Here solid lines are stable branches, while dashed and dashed-dot lines are unstable branches. The dashed-dot curve corresponds to unstable general travelling rolls. For any values of $G$ and $G_t$, inside (outside) $D(K_2)$, the solid curve corresponds to the standing (simple travelling) rolls, while the dashed curve corresponds to the simple travelling (standing) rolls. For $R < R_C$, the only stable solution is that of the conduction state represented by the solid line portion of the $R$-axis in figure 8. It is seen from this diagram that the oscillatory rolls are all supercritical and no sub-critical branch exists in the present problem.

## 6. Conclusion and some remarks

We have investigated the problem of nonlinear oscillatory convection in a horizontal mushy layer during alloy solidification. We analysed the two- and three-dimensional oscillatory modes of convection in the mushy layer using the model due to Amberg & Homsy (1993) and its extended form as studied by Anderson & Worster (1995). We performed a weakly nonlinear analysis to determine the finite-amplitude oscillatory solutions admitted by the nonlinear problem and carried out stability analyses to

determine the finite-amplitude solutions that are stable with respect to arbitrary three-dimensional disturbances. We found that all the three-dimensional finite-amplitude solutions in the form of travelling and standing waves are unstable. However, depending on the range of values of the parameters, two-dimensional finite-amplitude solutions in the form of either simple travelling rolls or standing rolls are found to be stable and, thus, preferred in a particular domain in the parameter space, while general travelling rolls were found to be unstable. We found that the simple travelling rolls are supercritical and stable over most of the domain in the parameter space. Standing rolls were also found to be supercritical but are stable only in a rather small region in the parameter space where the simple travelling rolls are unstable. No hysteretic effect and sub-critical solutions were found. Our results on the onset of plume convection and chimney formation within the mushy layer indicated that the chimney of the plume could be initiated internally or near the lower boundary. We found that the direction and the extent of chimneys can depend on the form of the preferred oscillatory rolls.

It should be noted that, as in the case of the stationary mode of convection noted by Anderson & Worster (1995), the quantitative conclusions of the present study may be altered by using a more sophisticated model such as a two-layer model of the type due to Worster (1992). For example, investigation of the present problem in a two-layer model of a liquid region overlying a mushy region may lead to the result that the stability boundary between the standing rolls and the simple travelling rolls may shift somewhat relative to the present result. However, the qualitative results of our studies, such as the preference of simple travelling rolls and standing rolls over the rest of the solutions should remain unchanged.

In the present work we identified a physical effect associated with the possibility of convection in the form of standing rolls, namely that due to the nonlinear permeability variations associated with the perturbations to the basic-state solid fraction. Based on this effect, our theory predicted stable standing rolls in a small region of the parameter space. In the absence of this physical effect, which is equivalent to the case of uniform permeability seen by the solidification system, simple travelling rolls are the only stable flow pattern throughout the entire ($G_t$, $G$)-plane.

Similar to the assumption of small $K_1$ made by Anderson & Worster (1995), we also considered a parameter regime, where in the present case $K_1 = O(\varepsilon)$, so that the stable solutions bifurcate supercritically. In the stationary convection case, Amberg & Homsy (1993) showed that when $K_1/C > 0.226$ the steady roll branch bifurcates subcritically. In the present work the assumption $K_1 = O(\varepsilon)$ does not allow any contribution of $K_1$ to the orders that are computed, but we speculate that the assumption of order-one values of $K_1$ may lead to the result that $R_{20} < 0$, which can be consistent with the similar physical effect as explained in Amberg & Homsy (1993) for the non-oscillatory convection case.

In regard to the range of values of the parameters $G$ and $G_t$ considered in this paper, it should be noted that, as also uncovered by Anderson & Worster (1996) from their linear results, the features of the oscillatory motion appeared to be explained more directly and easily as functions of $G$ and $G_t$ rather than $S$ and $C$. The range of values of $G$ and $G_t$ which were used to present the results in this paper, was found to correspond to the cases where the oscillatory modes can be distinctly identified and are preferred, in contrast to the non-oscillatory modes, which correspond to distinctly higher $R_C$ values. Although it has been of interest to consider the range of values of $G$ and $G_t$ which could cover those of the available experimental studies (Tait *et al.* 1992) ($G \approx 1.25$, $G_t \approx 0.04$), we found that such values of $G$ and $G_t$ lead

to a convection domain where the critical value of $R$ for the onset of oscillatory convection $R_C^{(o)}$, is too close to the critical value, of $R$ for the onset of stationary convection, $R_C^{(s)}$, and, hence, such values of $G$ and $G_t$ were not appropriate to present the results in this paper, though they are relevant for the results to be presented in the part 2.

The nonlinear study of stationary convection in mushy layers due to Anderson & Worster (1995) provided some results which helped to stimulate the present study and facilitated some of the selection of the parameter values for the present investigation. Anderson & Worster (1995) investigated possible stationary modes and solutions in the form of steady rolls and steady hexagons. They derived an evolution equation for the amplitude coefficients of such solutions, and their stability analysis for these solutions was based on that evolution equation. They considered the case of small $K_1$. Their analysis of the steady convection revealed the presence of an oscillatory instability, which was due to an unsuspected interaction between convection and solidification that can occur within the mushy layer. They reported that the point at which the coefficient of the time derivative term in their evolution equation vanishes corresponds to the appearance of the oscillatory mode at the minimum of the neutral stability curve for the real mode. However, their analysis treated only cases away from this point and considered only non-oscillatory solutions of their evolution equation in the form of steady rolls and steady hexagons. They also found that the existence of the oscillatory instability and the possibility of stable down-hexagons were associated with similar regions in the parameter space. They found that stable down-hexagons could not be obtained when $K_2 > 0.131$. It should be noted that the preference for stable down-hexagons has been of interest in relation to some available experimental evidence (Tait *et al.* 1992) where such flow pattern was observed in the flow of 28% ammonium chloride solution solidified from its base in a square tank. However, for the reasons stated in the previous paragraph, an appropriate model, which could be more relevant for comparison of its predicted results to those due to experimental observation, should take into account a combination of both oscillatory and non-oscillatory modes of convection in both nonlinear and stability analyses of the type carried out in the present paper. As stated in § 1, Part 2 takes into account the combination of both oscillatory and non-oscillatory modes and the results presented here form the basis for part 2.

An objective of part 2 is to determine the stable modes and their contributions to the preference of the experimentally observed down-hexagons (Tait *et al.* 1992). Some preliminary results of part 2 indicate that the contribution of the combination of two wavenumber vectors of the oscillatory modes and one wavenumber vector of the stationary modes to form the stable hexagons can enhance the preference for the down-hexagon regime much beyond that already detected in a stationary state system (Anderson & Worster 1995).

## Appendix A

The system of equations and boundary conditions at order $\varepsilon$ are given below

$$\Delta_2(-\nabla^2 V_{10} + R_{00}\theta_{10} + R_{10}\theta_{00}) = 0, \tag{A 1a}$$

$$\nabla^2\theta_{10} + G(R_{00}\Delta_2 V_{10} + R_{10}\Delta_2 V_{00} + R_{00}\boldsymbol{\Omega} V_{00}\cdot\nabla\theta_{00}) = 0, \tag{A 1b}$$

$$S\left[\left(\frac{\partial}{\partial t_1}\right)-\left(\frac{\partial}{\partial z}\right)\right]\phi_{10}+\nabla^2\theta_{10}+R_{00}\Delta_2 V_{10}$$

$$=-R_{10}\Delta_2 V_{00}-\left(S\frac{\omega_{11}}{\omega_{01}}\right)\frac{\partial\phi_{00}}{\partial t_1}+R_{00}\boldsymbol{\Omega}V_{00}\cdot\nabla\theta_{00}, \quad (A\,1c)$$

$$V_{10}=\theta_{10}=0 \quad \text{at} \quad z=0, \quad (A\,1d)$$

$$V_{10}=\theta_{10}=\phi_{10}=0 \quad \text{at} \quad z=1, \quad (A\,1e)$$

where

$$t_1=\omega t/\omega_{01}.$$

The solutions to the above system, which holds for $R_{10}=\omega_{11}=0$ (see § 3), are

$$(V_{10},\theta_{10},\phi_{10})=\sum_{l,p=-N}^{N}\{[\sin(2\pi z)F_1(\psi_{lp}),\sin(2\pi z)F_2(\psi_{lp}),\cos(2\pi z)F_3(\psi_{lp})]$$
$$\times(A_l^+\eta_l^++A_l^-\eta_l^-)(A_p^+\eta_p^++A_p^-\eta_p^-)+[0,0,\mathrm{i}\sin(2\pi z)F_4(\psi_{l,p})$$
$$\times(A_l^+\eta_l^++A_l^-\eta_l^-)(A_p^+\eta_p^+-A_p^-\eta_p^-)]\}, \quad (A\,2a)$$

where

$$\left.\begin{aligned}
\psi_{lp}&=\frac{\boldsymbol{a}_l\cdot\boldsymbol{a}_p}{\pi^2},\\
F_1(\psi_{lp})&=-(1-\psi_{lp})/[2\pi\sqrt{G(\psi_{lp}^2+4\psi_{lp}+7)}],\\
F_2(\psi_{lp})&=(1-\psi_{lp})(3+\psi_{lp})/(2\psi_{lp}^2+8\psi_{lp}+14),\\
F_3(\psi_{lp})&=[2\pi^3/(CG)](1-\psi_{lp})/[4\pi^2-\omega_{01}^2(S_l+S_p)^2],\\
F_4(\psi_{lp})&=[\pi^2/(CG)]\omega_{01}(1-\psi_{lp})(S_l+S_p)/[4\pi^2-\omega_{01}^2(S_l+S_p)^2].
\end{aligned}\right\} \quad (A\,2b)$$

The system of equations and boundary conditions at order $\varepsilon^2$ is

$$\left.\begin{aligned}
&\Delta_2(-\nabla^2V_{20}+R_{00}\theta_{20}+R_{20}\theta_{00})\\
&\quad=\left(\frac{\partial}{\partial z}\right)[\tilde{K}_1\boldsymbol{\Omega}V_{00}\cdot\nabla\phi_{00}+K_2\boldsymbol{\Omega}V_{00}\cdot\nabla(\phi_{00}^2)]\\
&\qquad+\nabla^2(\tilde{K}_1\phi_{00}\Delta_2V_{00}+K_2\phi_{00}^2\Delta_2V_{00}),\\
&\nabla^2\theta_{20}+G\Delta_2(R_{00}V_{20}+R_{20}V_{00})=GR_{00}(\boldsymbol{\Omega}V_{00}\cdot\nabla\theta_{10}+\boldsymbol{\Omega}V_{10}\cdot\nabla\theta_{00}),\\
&S\left(\frac{\partial}{\partial t_1}-\frac{\partial}{\partial z}\right)\phi_{20}+\Delta_2(R_{00}V_{20}+R_{20}V_{00})+\nabla^2\theta\\
&\quad=-\left(S\frac{\omega_{21}}{\omega_{01}}\right)\frac{\partial\phi_{00}}{\partial t_1}+R_{00}(\boldsymbol{\Omega}V_{00}\cdot\nabla\theta_{10}+\boldsymbol{\Omega}V_{10}\cdot\nabla\theta_{00}),\\
&\theta_{20}=V_{20}=0 \quad \text{at} \quad z=0,\ \theta_{20}=V_{20}=\phi_{20}=0 \quad \text{at} \quad z=1,
\end{aligned}\right\} \quad (A\,3)$$

where $\tilde{K}_1=K_1/\varepsilon$ is an order-one constant.

The expressions for $T_{nm}^{(j)}(j=1,\ldots,8)$ introduced in (16$a$) and (16$b$) are

$$T_{nm}^{(1)}=(H_{-n,n,n}+H_{n,-n,n})\delta_{nm}+(H_{n,n,-n})\delta_{n,-m}$$
$$+(H_{-m,n,m}+H_{n,-m,m}+H_{m,-m,n})(1-\delta_{nm})(1-\delta_{n,-m}), \quad (A\,4a)$$

$$T^{(2)}_{nm} = (H^*_{-n,n,n} + H^*_{n,-n,n})\delta_{nm} + (H^*_{n,n,-n})\delta_{n,-m} + (H^*_{-m,n,m} + H^*_{n,-m,m} + H^*_{m,-m,n})(1-\delta_{nm})(1-\delta_{n,-m}), \quad (A\,4b)$$

$$T^{(3)}_{nm} = (\tilde{H}_{-n,n,n} + \tilde{H}^*_{n,-n,n})\delta_{nm} + (\tilde{H}_{n,n,-n})\delta_{n,-m} + (\tilde{H}_{-m,n,m} + \tilde{H}^*_{n,-m,m} + H^*_{m,-m,n})(1-\delta_{nm})(1-\delta_{n,-m}), \quad (A\,4c)$$

$$T^{(4)}_{nm} = (\tilde{H}^*_{-n,n,n} + \tilde{H}_{n,-n,n})\delta_{nm} + (\tilde{H}^*_{n,n,-n})\delta_{n,-m} + (\tilde{H}^*_{-m,n,m} + \tilde{H}_{n,-m,m} + \tilde{H}_{m,-m,n})(1-\delta_{nm})(1-\delta_{n,-m}), \quad (A\,4d)$$

$$T^{(5)}_{nm} = (H_{-n,n,n} + H_{n,-n,n})\delta_{nm} + (H_{n,n,-n})\delta_{n,-m} + (H_{-m,n,m} + H_{n,-m,m} + \tilde{H}_{m,-m,n})(1-\delta_{nm})(1-\delta_{n,-m}), \quad (A\,4e)$$

$$T^{(6)}_{nm} = (\tilde{H}_{-n,n,n} + \tilde{H}^*_{n,-n,n})\delta_{nm} + (\tilde{H}_{n,n,-n})\delta_{n,-m} + (\tilde{H}_{-m,n,m} + \tilde{H}^*_{n,-m,m} + \tilde{H}^*_{m,-m,n})(1-\delta_{nm})(1-\delta_{n,-m}), \quad (A\,4f)$$

$$T^{(7)}_{nm} = (H^*_{-n,n,n} + H^*_{n,-n,n})\delta_{nm} + (H^*_{n,n,-n})\delta_{n,-m} + (H^*_{-m,n,m} + H^*_{n,-m,m} + H^*_{m,-m,n})(1-\delta_{nm})(1-\delta_{n,-m}), \quad (A\,4g)$$

$$T^{(8)}_{nm} = (\tilde{H}^*_{-n,n,n} + \tilde{H}_{n,-n,n})\delta_{nm} + (\tilde{H}^*_{n,n,-n})\delta_{n,-m} + (\tilde{H}^*_{-m,n,m} + \tilde{H}_{n,-m,m} + H_{m,-m,n})(1-\delta_{nm})(1-\delta_{n,-m}). \quad (A\,4h)$$

where

$$H_{lmp} = [\pi^2/(2\sqrt{G})](2+\psi_{lm}+\psi_{pm})F_2(\psi_{lp}) + \pi^3(1+\psi_{lp}+\psi_{lm}+\psi_{pm}) \times F_1(\psi_{lp}) + (K_2\pi/\sqrt{G})[(2+\psi_{lp}+\psi_{lm}+2\psi_{pm})F_6(S_l,S_p) - (\psi_{lm}+\psi_{pm})F_5(S_l,S_p) + (1/\pi)F_7(S_l,S_p), \quad (A\,4i)$$

$$F_5(S_l,S_p) = \langle \cos(2\pi z) f_l(z) f_p(z)\rangle, \quad (A\,4j)$$

$$F_6(S_l,S_p) = \langle f_l(z) f_p(z)\rangle, \quad (A\,4k)$$

$$F_7(S_l,S_p) = \langle \sin(2\pi z) f_p(z)(\mathrm{d}/\mathrm{d}z) f_l(z)\rangle. \quad (A\,4l)$$

The expression for $\tilde{H}_{lmp}$ is the same as that for $H_{lmp}$, provided $f_l(z)$ is replaced by $f^*_l(z)$.

## Appendix B

The solutions to the system of equations and boundary conditions for disturbances at order $\varepsilon$ are

$$V'_{10} = 2\sin(2\pi z) \sum_{l=-\infty,p=-N}^{l=\infty,p=N} F_1(\psi_{lp})(\tilde{A}^+_l \eta^+_l + \tilde{A}^-_l \eta^-_l)(A^+_p \eta^+_p + A^-_p \eta^-_p), \quad (B\,1a)$$

$$\theta'_{10} = 2\sin(2\pi z) \sum_{l=-\infty,p=-N}^{l=\infty,p=N} F_2(\psi_{lp})(\tilde{A}^+_l \eta^+_l + \tilde{A}^-_l \eta^-_l)(A^+_p \eta^+_p + A^-_p \eta^-_p), \quad (B\,1b)$$

$$\phi'_{10} = 2\cos(2\pi z) \sum_{l=-\infty,p=N}^{l=\infty,p=N} F_3(\psi_{lp})(\tilde{A}_l^+\eta_l^+ + \tilde{A}_l^-\eta_l^-)(A_p^+\eta_p^+ + A_p^-\eta_p^-) + 2\mathrm{i}$$

$$\times \sin(2\pi z) \sum_{l=-\infty,p=-N}^{l=\infty,p=N} F_4(\psi_{lp})(\tilde{A}_l^+\eta_l^+ + \tilde{A}_l^-\eta_l^-)(A_p^+\eta_p^+ - A_p^-\eta_p^-). \quad (\mathrm{B}\,1c)$$

The system for disturbances at order $\varepsilon^2$ is

$$\Delta_2(-\nabla^2 V'_{20} + R_{00}\theta'_{20} + R_{20}\theta'_{00})$$
$$= (\partial/\partial z)[\tilde{K}_1(\boldsymbol{\Omega}V'_{00}\cdot\nabla\phi_{00} + \boldsymbol{\Omega}V_{00}\cdot\nabla\phi'_{00}) + K_2(\boldsymbol{\Omega}V'_{00}\cdot\nabla(\phi_{00}^2)$$
$$+ 2\boldsymbol{\Omega}V_{00}\cdot\nabla(\phi'_{00}\phi_{00}))] + \nabla^2[\tilde{K}_1(\phi'_{00}\Delta_2 V_{00} + \phi_{00}\Delta_2 V'_{00})$$
$$+ K_2(2\phi'_{00}\phi_{00}\Delta_2 V_{00} + \phi_{00}^2\Delta_2 V'_{00})], \quad (\mathrm{B}\,2a)$$

$$\nabla^2\theta'_{20} + G\Delta_2(R_{00}V'_{20} + R_{20}V'_{00})$$
$$= GR_{00}(\boldsymbol{\Omega}V'_{00}\cdot\nabla\theta_{10} + \boldsymbol{\Omega}V_{00}\cdot\nabla\theta'_{10} + \boldsymbol{\Omega}V'_{10}\cdot\nabla\theta_{00}$$
$$+ \boldsymbol{\Omega}V_{10}\cdot\nabla\theta'_{00}) + \sigma_{20}\theta'_{00} + [(1-G)/G]\phi'_{2(-1)}, \quad (\mathrm{B}\,2b)$$

$$S\left(\frac{\partial}{\partial t_1} - \frac{\partial}{\partial z}\right)\phi'_{20} + S\sigma_{20}\phi'_{00} + \Delta_2(R_{00}V'_{20} + R_{20}V'_{00}) + \nabla^2\theta'_{20}$$
$$= -S\left(\frac{\omega_{21}}{\omega_{01}}\right)\frac{\partial\phi'_{00}}{\partial t_1} + R_{00}(\boldsymbol{\Omega}V'_{00}\cdot\nabla\theta_{10} + \boldsymbol{\Omega}V_{00}\cdot\nabla\theta'_{10} + \boldsymbol{\Omega}V'_{10}\cdot\nabla\theta_{00} + \boldsymbol{\Omega}V_{10}\cdot\nabla\theta'_{00}), \quad (\mathrm{B}\,2c)$$

$$\theta'_{20} = V'_{20} = 0 \quad \text{at} \quad z = 0,\ \theta'_{20} = V'_{20} = \phi'_{20} = 0 \quad \text{at} \quad z = 1. \quad (\mathrm{B}\,2d)$$

The solvability conditions for the disturbance system at order $\varepsilon^2$ are reduced to the following set of equations:

$$(2R_{20} - S_0\sigma_{20})|\tilde{A}_n^{\pm}|$$
$$= \sum\{\langle(\tilde{A}_n^{\pm}\eta_n^{\pm} + \tilde{A}_{-n}^{\pm}\eta_{-n}^{\pm})[A_p^+\eta_p^+(\tilde{A}_m^+\eta_m^+ + \tilde{A}_m^-\eta_m^-)(H_{lmp}A_l^+\eta_l^+ + \tilde{H}_{lmp}A_l^-\eta_l^-)$$
$$+\tilde{A}_p^+\eta_p^+(A_m^+\eta_m^+ + A_m^-\eta_m^-)(H_{lmp}A_l^+\eta_l^+ + \tilde{H}_{lmp}A_l^-h_l^-) + A_p^+\eta_p^+(A_m^+\eta_m^+ + A_m^-\eta_m^-)$$
$$\times(H_{lmp}\tilde{A}_l^+\eta_l^+ + \tilde{H}_{lmp}\tilde{A}_l^-\eta_l^-) + A_p^-\eta_p^-(\tilde{A}_m^+\eta_m^+ + \tilde{A}_m^-\eta_m^-)(\tilde{H}_{lmp}^*A_l^+\eta_l^+ + H_{lmp}^*A_l^-\eta_l^-)$$
$$+\tilde{A}_p^-\eta_p^-(A_m^+\eta_m^+ + A_m^-\eta_m^-)(\tilde{H}_{lmp}^*A_l^+\eta_l^+ + H_{lmp}^*A_l^-\eta_l^-)$$
$$+A_p^-\eta_p^-(A_m^+\eta_m^+ + A_m^-\eta_m^-)(\tilde{H}_{lmp}^*\tilde{A}_l^+\eta_l^+ + H_{lmp}^*\tilde{A}_l^-\eta_l^-)]\rangle\}, \quad (\mathrm{B}\,3a)$$

where

$$S_0 = 2\tilde{S}_0/(\pi G\sqrt{G}) \quad (\mathrm{B}\,3b)$$

and

$$\tilde{S}_0 = -1 + [4\pi^2 G_t/(\pi^2 - \omega_{01}^2)^2][\pi^2 + \omega_{01}^2 + 2\pi^2\cos(\omega_{01}) + 8\pi^2\omega_{01}\sin(\omega_{01})/(\pi^2 - \omega_{01}^2)]. \quad (\mathrm{B}\,3c)$$

The result of our calculation of the coefficient $S_0$ indicated that it is always positive, increases with $G_t$ and decreases with increasing $G$.

The solvability conditions for the system of inclined disturbances at order $\varepsilon^2$ are reduced to the following set of equations:

$$
\begin{aligned}
&(2R_{20} - S_0\sigma_{20})|\tilde{A}_r^{\pm}|^2 \\
&\quad = \sum \{\langle (\tilde{A}_r^{\pm}\tilde{\eta}_r^{\pm} + \tilde{A}_{-r}^{\pm}\tilde{\eta}_{-r}^{\pm})[A_p^+\eta_p^+(\tilde{A}_m^+\tilde{\eta}_m^+ + \tilde{A}_m^-\tilde{\eta}_m^-)(H_{lmp}A_l^+\eta_l^+ + \tilde{H}_{lmp}A_l^-\eta_l^-) \\
&\qquad + \tilde{A}_l^+\tilde{\eta}_l^+(A_m^+\eta_m^+ + A_m^-\eta_m^-)(H_{lmp}A_l^+\eta_l^+ + \tilde{H}_{lmp}A_l^-\eta_l^-) \\
&\qquad + A_p^+\eta_p^+(A_m^+\eta_m^+ + A_m^-\eta_m^-)(H_{lmp}\tilde{A}_l^+\tilde{\eta}_l^+ + \tilde{H}_{lmp}\tilde{A}_l^-\tilde{\eta}_l^-) + A_p^-\eta_p^-(\tilde{A}_m^+\tilde{\eta}_m^+ + \tilde{A}_m^-\tilde{\eta}_m^-) \\
&\qquad \times(\tilde{H}_{lmp}^*A_l^+\eta_l^+ + H_{lmp}^*A_l^-\eta_l^-) + \tilde{A}_p^-\tilde{\eta}_p^-(A_m^+\eta_m^+ + A_m^-\eta_m^-)(\tilde{H}_{lmp}^*A_l^+\eta_l^+ \\
&\qquad + H_{lmp}^*A_l^-\eta_l^-) + A_p^-\eta_p^-(A_m^+\eta_m^+ + A_m^-\eta_m^-)(\tilde{H}_{lmp}^*\tilde{A}_l^+\tilde{\eta}_l^+ + H_{lmp}^*\tilde{A}_l^-\tilde{\eta}_l^-)\rangle\}. \qquad \text{(B 4)}
\end{aligned}
$$

## REFERENCES


Amberg, G. & Homsy, G. M. 1993 Nonlinear analysis of buoyant convection in binary solidification with application to channel formation. *J. Fluid Mech.* **252**, 79–98.

Anderson, D. M. & Worster, M. G. 1995 Weakly nonlinear analysis of convection in mushy layers during the solidification of binary alloys. *J. Fluid Mech.* **302**, 307–331.

Anderson, D. M. & Worster, M. G. 1996 A new oscillatory instability in a mushy layer during the solidification of binary alloys. *J. Fluid Mech.* **307**, 245–267.

Busse, F. H. 1967 The stability of finite amplitude convection and its relation to an extremum principal. *J. Fluid Mech.* **30**, 625–649.

Busse, F. H. & Riahi, D. N. 1980 Nonlinear convection in a layer with nearly insulating boundaries. *J. Fluid Mech.* **96**, 243–256.

Chandrasekhar, S. 1961 *Hydrodynamic and Hydromagnetic Stability*. Clarendon.

Chen, F., Lu, J. W. & Yang, T. L. 1994 Convective instability in ammonium chloride solution directionally solidified from below. *J. Fluid Mech.* **276**, 163–187.

Chung, C. A. & Chen, F. 2000 Onset of plume convection in mushy layers. *J. Fluid Mech.* **408**, 53–82.

Fowler, A. C. 1985 The formation of freckles in binary alloys. *IMA J. Appl. Maths* **35**, 159–174.

Guba, P. 2001 On the finite-amplitude steady convection in rotating mushy layers. *J. Fluid Mech.* **437**, 337–365.

Joseph, D. D. 1976 *Stability of Fluid Motions*. Springer.

Neilson, D. G. & Incropera, F. P. 1993 Effect of rotation on fluid motion and channel formation during unidirectional solidification of a binary alloy. *Intl J. Heat Mass Transfer* **36**, 489–505.

Riahi, D. N. 1992 Weakly nonlinear oscillatory convection in a rotating fluid. *Proc. R. Soc. Lond.* A **436**, 33–54.

Riahi, D. N. 2002 On nonlinear convection in mushy layers. Part 2. Mixed oscillatory and stationary modes of convection. In preparation.

Sayre, T. L. & Riahi, D. N. 1995 Oscillatory instabilities of the liquid and mushy layers during solidification of alloys under rotational constraint. *TAM Rep.* 808 UILU-ENG-95.

Sayre, T. L. & Riahi, D. N. 1997 Oscillatory instability of the liquid and mushy regions during solidification of alloys under rotational constraint. *Acta Mechanica* **121**, 143–152.

Schluter, A., Lortz, D. & Busse, F. H. 1965 On the stability of finite amplitude convection. *J. Fluid Mech.* **23**, 129–144.

Schulze, T. P. & Worster, M. G. 1999 Weak convection, liquid inclusions and the formation of chimneys in mushy layers. *J. Fluid Mech.* **388**, 197–215.

Tait, S., Jahrling, K. & Jaupart, C. 1992 The planform of compositional convection and chimney formation in a mushy layer. *Nature* **359**, 406–408.

Worster, M. G. 1992 Instabilities of the liquid and mushy regions during solidification of alloys. *J. Fluid Mech.* **237**, 649–669.

# CORRIGENDUM

On nonlinear convection in mushy layers. Part 1. Oscillatory modes of convection

By D. N. Riahi

*Journal of Fluid Mechanics*, vol. 467 (2002), pp. 331–359

A reader trying to reproduce or extend the calculations in this paper should be aware that the author omitted to mention simple rescaling applied to $R_{10}$, $R_{20}$, $\omega_{11}$, $K_1$, and $K_2$. All the presentation and discussion that referred to these quantities was for the actual values divided by $\pi$ (i.e. $R_{10}/\pi$, $R_{20}/\pi$, etc.).

# CORRIGENDUM

On nonlinear convection in mushy layers. Part 1. Oscillatory modes of convection

By D. N. Riahi

*Journal of Fluid Mechanics*, vol. 467 (2002), pp. 331–359

The paper presents various analytical expressions relating to coefficients in small-amplitude evolution equations for convection in mushy layers. Some of the deductions and graphical illustrations were made using inadequate numerical precision, which led to erroneous deductions. In particular, equation (13*a*) is singular at $\omega_{01} = \pi$, and care is needed when using it to determine $G_t$ in the neighbourhood of the singularity. As $\omega_{01} \to \pi$

$$R_{01} \sim 3\pi G_t \sqrt{G}/4,$$

which illustrates in particular that the singularity is removable. The numerical error made in simply taking $\pi = 3.14$ shows up in figures 1–7, which are reproduced here in corrected form, numbered C1–C7. Note the change of scale of the ordinate in figures 2, 3, 4, 6, and 7 compared to the original versions.

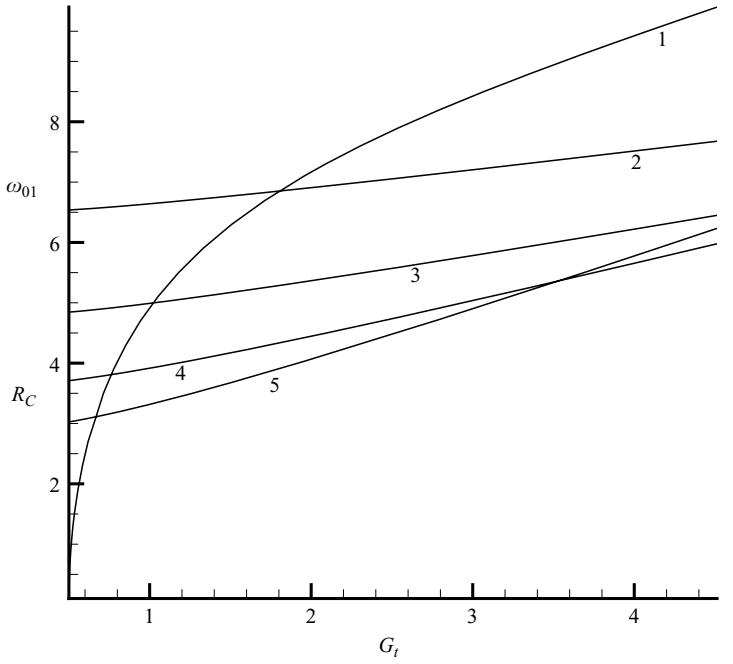


FIGURE C1. The frequency $\omega_{01}$ and the critical value of the scaled Rayleigh number $R_C$ versus $G_t$. The curve labelled 1 shows $\omega_{01}$. Curves 2, 3, 4 and 5 show $R_C$ and correspond, respectively, to $G = 1.01, 2.0, 4.0$ and $8.0$.

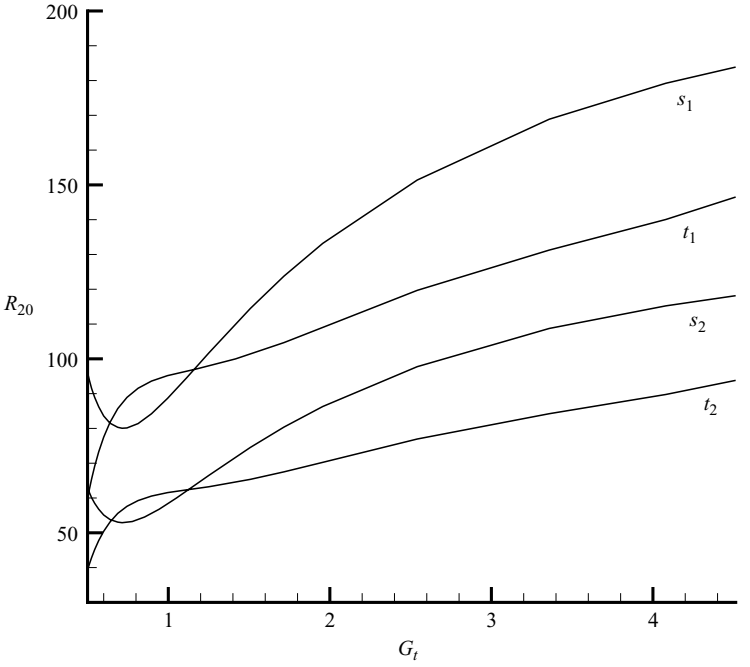


FIGURE C2. $R_{20}$ versus $G_t$ for rolls. $R_{20}$ for standing rolls ($s$) and simple travelling rolls ($t$) is plotted for $G = 2.0$ and $K_2 = 0.1571$ ($s_1, t_1$), and for $G = 4.0$ and $K_2 = 0.3142$ ($s_2, t_2$).

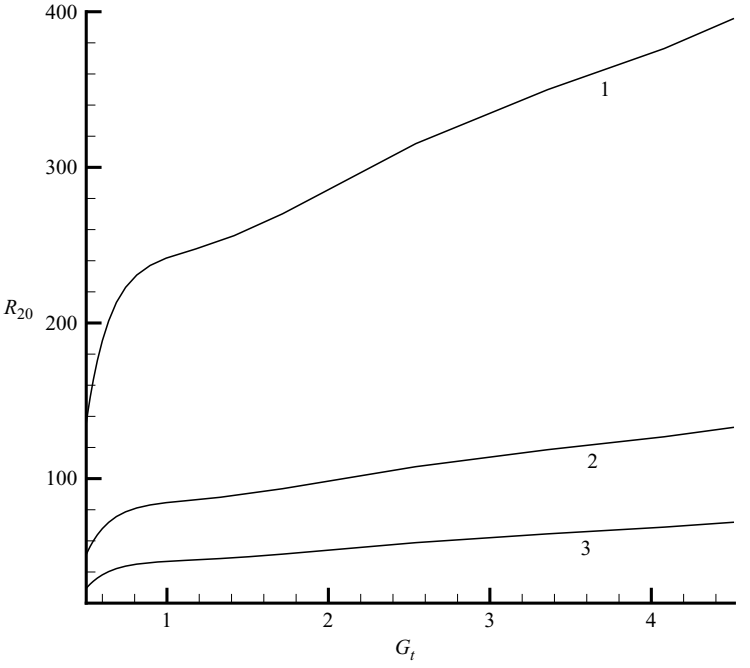


FIGURE C3. $R_{20}$ versus $G_t$ for simple travelling rolls. $K_2 = 0.4712$ and graphs labelled 1, 2 and 3, present, respectively, $R_{20}^{(st)}$ for $G = 2.0, 4.0$ and 8.0.

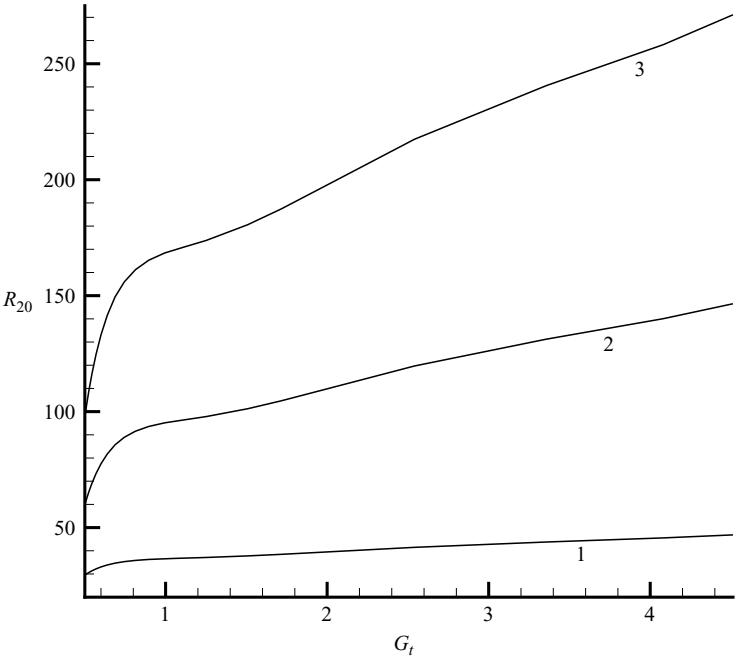


FIGURE C4. $R_{20}$ versus $G_t$ for simple travelling rolls. $G = 2.0$ and graphs labelled 1, 2 and 3 present, respectively, $R_{20}^{(st)}$ for $K_2 = 0.0314, 0.1571$ and $0.3142$.

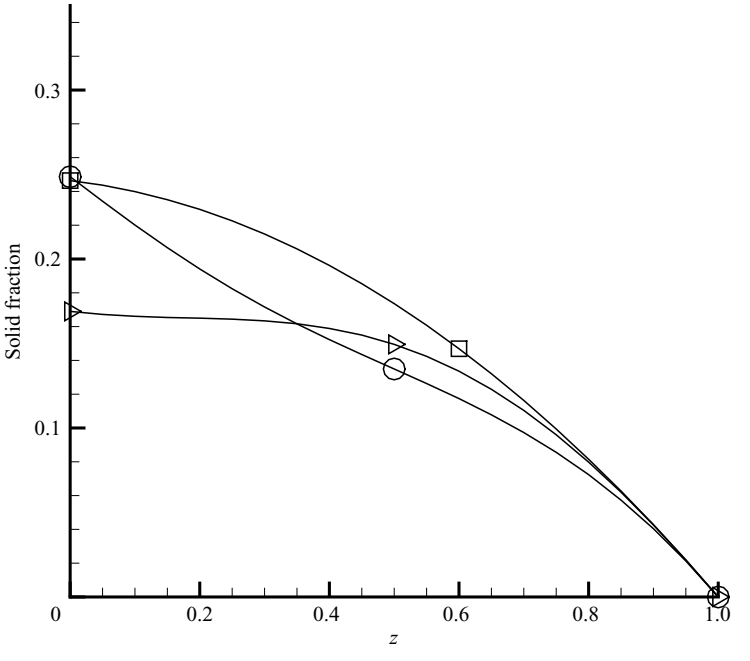


FIGURE C5. Solid fraction for standing rolls versus $z$ for $G = 2.0$, $K_2 = 0$ and $G_t = 0.7$. Here graphs labelled by the square, circle and triangle symbols show, respectively, the basic solid fraction $\phi_B$, $\tilde{\phi}(y = 0, z, t = 0)$ and $\tilde{\phi}(y = 0, z, t = 0.5)$.

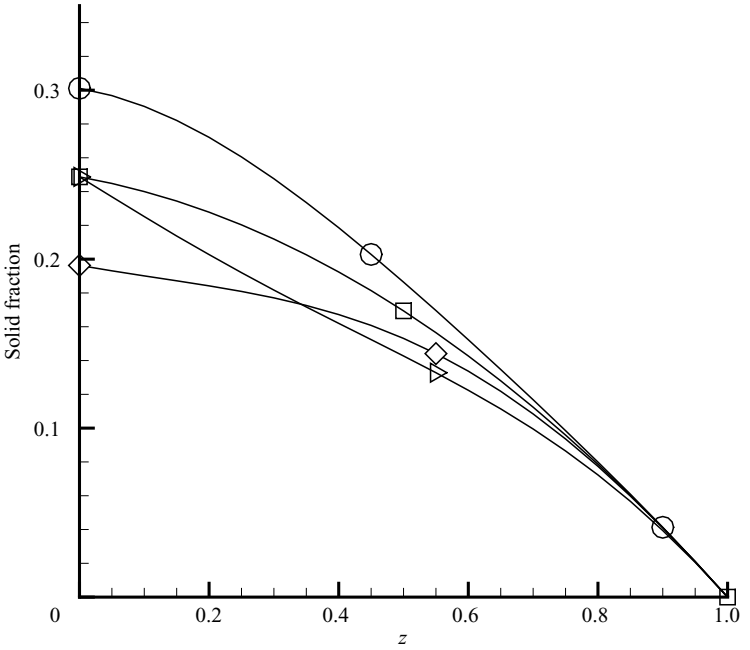


FIGURE C6. Solid fraction for simple travelling rolls versus $z$ for $G = 2.0$, $K_2 = 0$ and $G_t = 0.67$. Here graphs labelled by the square, circle, triangle and diamond symbols show, respectively, $\phi_B$, $\tilde{\phi}(y = 0.5, z, t = 0)$, $\tilde{\phi}(y = 0.5, z, t = 0.5)$ and $\tilde{\phi}(y = 0, z, t = 0.5)$.

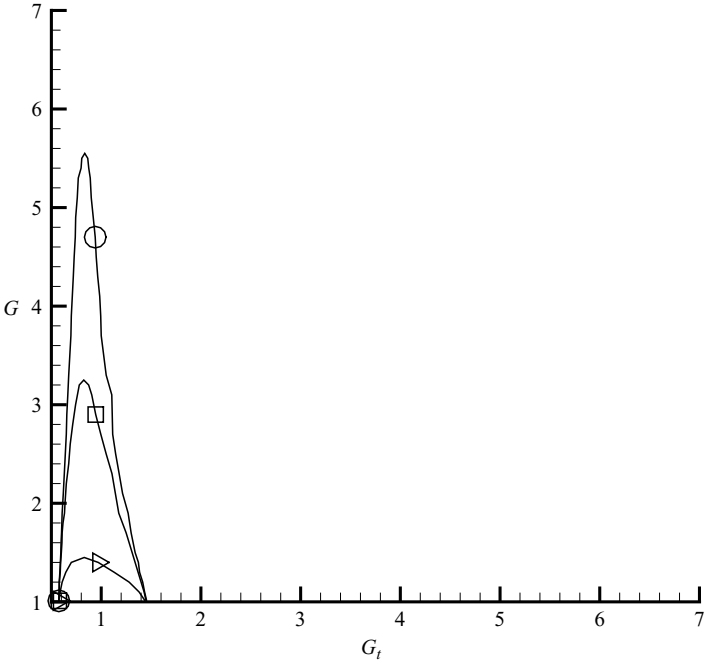


FIGURE C7. Regions of stable and preferred oscillatory modes of convection in the $(G_t, G)$-plane for different values of $K_2$. The stability boundaries labelled by the circle, square and triangle symbols correspond, respectively, to $K_2 = 0.2199, 0.1671$ and $0.0314$. For a given $K_2$ standing rolls are stable in the small region bounded by the stability curve, while simple travelling rolls are stable outside that region.